bioRxiv preprint doi: https://doi.org/10.1101/109785; this version posted February 19, 2017. The copyright holder for this preprint (which was not certified by peer review) is the author/funder. All rights reserved. No reuse allowed without permission.

Constraining CD45 exclusion at close-contacts provides a mechanism for discriminatory T-cell receptor signalling

Ricardo A Fernandes*[1,7], Kristina A Ganzinger*[2,8], Justin Tzou[5], Peter Jönsson[2,9], Steven F Lee[2], Matthieu Palayret[2], Ana Mafalda Santos[1], Veronica T Chang[1,10], Charlotte Macleod[2], B. Christoffer Lagerholm[1], Alan E. Lindsay[4], Omer Dushek[3], Andreas Tilevik[6,§], Simon J Davis[1,§], David Klenerman[2,§]

* These authors contributed equally to the work
§ Correspondence: andreas.tilevik@his.se, simon.davis@imm.ox.ac.uk, dk10012@cam.ac.uk
Lead contact author: dk10012@cam.ac.uk

[1] Radcliffe Department of Medicine and MRC Human Immunology Unit, John Radcliffe Hospital, University of Oxford, Oxford OX3 9DS, United Kingdom

[2] Department of Chemistry, University of Cambridge, Cambridge, CB2 1EW, United Kingdom

[3] Sir William Dunn School of Pathology, University of Oxford, Oxford, UK; Wolfson Centre for Mathematical Biology, University of Oxford, Oxford, UK.

[4] Department of Applied and Computational Mathematics and Statistics, University of Notre Dame, Notre Dame, IN, USA, 46556.

[5] Mathematics Department, University of British Columbia, Vancouver, BC, V6T 1Z2, Canada.

[6] School of Bioscience, University of Skövde, 541 28 Skövde, Sweden

[7] Present address: Depts. of Molecular and Cellular Physiology, and Structural Biology, Stanford University, CA 94305, US
[8] Present address: Max-Planck-Institut für Biochemie (MPI for Biochemistry), 82152 Martinsried, Germany.
[9] Present address: Department of Chemistry, Lund University, SE-22100 Lund, Sweden
[10] Present address: Division of Structural Biology, Wellcome Trust Centre for Human Genetics, University of Oxford, Oxford OX3 7BN

Keywords: T-cell receptor/receptor triggering/single-molecule imaging/CD45/Cell topography/dwell-time

bioRxiv preprint doi: https://doi.org/10.1101/109785; this version posted February 19, 2017. The copyright holder for this preprint (which was not certified by peer review) is the author/funder. All rights reserved. No reuse allowed without permission.

Summary

The T-cell receptor (TCR) must discriminate between peptides bound to major histocompatibility complex proteins and yet it can be triggered even without ligands at close contacts characterized by local depletion of the phosphatase, CD45. Here, we use a quantitative treatment of signaling that incorporates moving-boundary passage time calculations and is reliant only upon receptor dwell-time at close contacts to reconcile the contradictory properties of TCR triggering. We validate the model by showing that signaling is inversely related to close contact growth-rate and sensitive to the local balance of kinase and phosphatase activities. The model predicts that the small size of close contacts imposed by cell topography, and their short duration owing to the destabilizing effects of, for example, the glycocalyx, crucially underpins ligand discrimination by T cells without recourse to classical proofreading schemes. Based on simple physical principles, therefore, our model accounts for the main features of TCR triggering.

Introduction

Triggering of the T-cell receptor (TCR) following binding to peptide-MHC complexes (pMHC) on antigen-presenting cells (APCs) sets T cells on course to responding to pathogens and tumors (Smith-Garvin et al., 2009). Inefficient pMHC discrimination may lead to immunodeficiency or autoimmunity. TCR triggering is very sensitive, selective and fast: binding to a single pMHC is sufficient to induce TCR triggering, that is, increased tyrosine phosphorylation of signaling motifs located within the cytoplasmic domains of the CD3 subunits associated with the TCRαβ heterodimer, within seconds of pMHC binding (Huang et al., 2013; Irvine et al., 2002; Purbhoo et al., 2004). However, the mechanistic basis of TCR sensitivity and specificity is still poorly understood (for a detailed review see Chakraborty and Weiss, 2014).

The kinetic-segregation (KS) model proposes that in resting T-cells, TCR phosphorylation by kinases is kept in check by the counter-activity of large phosphatases (CD45; Davis and van der Merwe, 2006). This equilibrium is perturbed when contacts are formed between T cells and APCs that exclude the receptor-type protein tyrosine phosphatase CD45, resulting in net receptor phosphorylation. Recently, Chang et al. (2016) showed that CD45 spontaneously segregates from the TCR and Lck present in close contacts that are created when T cells interact with artificial and model cell surfaces. In agreement with predictions of the KS model, TCR triggering was observed under these conditions even when receptor ligands were absent. These findings suggested that TCR triggering is not explicitly ligand dependent, *i.e.* reliant on *e.g.* conformational changes or oligomerization, or on mechanical forces acting through the TCR. However, the work of Chang et al. introduced a new problem insofar as it was unclear what it is that allows T-cells to respond to, and to discriminate between, cognate ligands. One possibility is that interactions with ligands influence the dwell-time of the TCR in CD45-depleted close contacts, and that other factors underpin ligand discrimination.

bioRxiv preprint doi: https://doi.org/10.1101/109785; this version posted February 19, 2017. The copyright holder for this preprint (which was not certified by peer review) is the author/funder. All rights reserved. No reuse allowed without permission.

But what could these factors be? Historically, TCR triggering was assumed to rely exclusively on pMHC binding and, in modeling the process, little consideration is usually given to the structure or dynamics of the contacts formed between T cells and APCs. Importantly, encounters between T-cells and APCs are known to be transient and several reports indicate that initial close contacts are only sub-μm in size (Sage et al., 2012; Stoll et al., 2002). In contrast, the model surfaces often used to study the early and late stages of T-cell activation, including protein-coated glass surfaces and supported lipid bilayers (SLBs), tend to favor the formation of stable and large cellular contacts (Grakoui et al., 1999; Groves and Dustin, 2003). Moreover, although it is known that heavily glycosylated proteins such as CD43 influence both T-cell contact formation and TCR signaling (Ardman et al., 1992; Manjunath et al., 1993, 1995; Mazurov et al., 2012), these proteins are not routinely incorporated into model surfaces. In addition, adhesion proteins such as CD2 that are likely to profoundly affect contact structure and to facilitate the scanning of pMHCs for cognate peptides (van der Merwe *et al.* 1995) are usually left out of the experiments. Finally, the actual role of integrins in mediating close contact formation is unclear given that the activities of integrins themselves are affected by receptor signaling (Dustin and Springer, 1989; Kinashi, 2005). At present, therefore, we have a very limited understanding of whether or how the structure and dynamics of contact formation influence TCR signaling *per se*, and especially ligand discrimination.

Here, we undertake a quantitative analysis of signaling initiated when T cells interact with surfaces lacking TCR ligands, using single-molecule imaging to characterize the behavior of CD45, Lck and the TCR, and calcium reporters to simultaneously monitor cellular responses. We develop a new theoretical treatment of T-cell signaling utilizing moving-boundary passage time calculations that is reliant only upon TCR occupancy of close contacts from which CD45 is depleted, and that we validate by showing that signaling lag-time is inversely related to close contact growth-rate. Our model allows signaling to occur ligand independently and identifies conditions that might even reinforce signaling by increasing the fraction of triggered receptors beyond those bound by ligands. Most importantly, ligand discrimination emerges as a robust consequence of topography-based dwell-time modulation at close contacts, without recourse to conventional proof-reading schemes. A theory of signaling contingent only upon receptor occupancy of phosphatase-depleted close contacts, therefore, accounts for the main features of TCR triggering.

Results

Single-molecule behavior of CD45, Lck and TCR at close contacts

The goal of this study was to understand how an intrinsically ligand-independent triggering mechanism discriminates between ligands. To this end, we developed and tested a new theoretical treatment of T-cell signaling contingent only upon TCR occupancy close contacts. To parameterize variables used in the model, we analyzed the diffusion and distribution of key signaling molecules during the earliest stages of close contact formation as T cells spread on IgG-coated glass surfaces and SLBs. We used two-color total internal reflection fluorescence (TIRF) microscopy to localize close contacts and to

bioRxiv preprint doi: https://doi.org/10.1101/109785; this version posted February 19, 2017. The copyright holder for this preprint (which was not certified by peer review) is the author/funder. All rights reserved. No reuse allowed without permission.

simultaneously track CD45, Lck and TCR at the single-molecule level. To achieve this, we used high-density labeling of CD45 to define the boundaries of the close contacts and sub-stoichiometric labeling of Lck, TCR or CD45 (**Figure 1A**). For T cells interacting with IgG-coated glass surfaces, 96.8±0.1% of CD45 molecules were excluded from the close contacts (**Figure 1B,** and **Table S1**). An extracellular domain (ECD)-truncated form of CD45 (HA-CD45) was less excluded (86±2%; **Figure S1A** and **Table S1**). While 6±1% of wild-type Lck was found inside the close contacts (**Figure 1C** and **Table S1**), this fraction increased to 33±3% when residues involved in Lck-CD4 pairing were mutated (mLck; Kim et al., 2003; **Table S1**), suggesting that the exclusion of Lck is at least partially dependent on its association with CD4. Only 5±2% of all detected TCRs were in close contacts (**Figure 1D**, **Table S1** and **Movie S1**). The high levels of protein segregation observed for CD45, Lck/CD4 and the TCR suggest that the contacts formed between T cells and protein-coated glass surfaces are narrow enough to exclude large fractions of all proteins with extracellular regions $\geq$75 Å. Close contacts are dynamic structures and the initial small multifocal contacts were observed to merge into single larger contacts (**Movie S2** and **Figure S1B and S1C**). T-cell close contact growth over time therefore results in increasingly larger CD45-depleted regions.

To create contacts with defined separation of the T cell- and model-surfaces like those expected to form *in vivo*, we used supported lipid bilayers (SLBs) wherein contact formation was initiated by rCD2-rCD48 interactions (Chang et al., 2016). Jurkat T-cells expressing signaling-deficient, CD48-T92A were allowed to settle on SLBs presenting rCD2 (CD48TM-T92A binds rCD2 with a K_d of ~11 uM, similar to the hCD58/CD2 interaction; Evans et al., 2006). In these experiments, CD45, Lck and TCR segregation from close contacts was reduced compared to that for T-cell interactions with glass surfaces (**Figure 1H** and **Table S2**). Nevertheless, CD45 still exhibited the strongest segregation: 13±3% of CD45 molecules were found inside the close contacts (**Figure 1E**), versus 56±7% and 40±6% of Lck and TCR proteins, respectively (**Figures 1F and 1G**). Despite the differences in their exclusion from contacts formed on glass or SLBs, the ratio of CD45 to Lck inside the close contacts was similar between the two model surfaces, *i.e.* approximately 2:1 on SLBs and 2.5:1 on IgG-coated glass. The initial CD45/Lck ratio of 5 to 1 at the unperturbed T-cell surface was thereby reduced by ~50% (**Figure S2A;** Chang et al., 2016).

Quantitative analysis of CD45, Lck and TCR motion for cells interacting with the SLBs revealed that TCR diffusion was ~2-fold slower compared to CD45 and Lck, and that the mean diffusion coefficients for molecules diffusing inside and outside the contacts were similar (**Figure 1H** and **Figure S2B**). Stochastic optical reconstruction microscopy (**Figures 1I** and **S3A, S3B**) revealed that CD45 exclusion is not contact-size dependent, as CD45 was excluded from all contacts including those with sizes smaller than the diffraction limit (~80 nm). Because these contacts were formed within seconds of T-cell/surface interaction, this suggests that CD45 segregation occurs simultaneously with close contact formation. CD45 segregation also occurred independently of active cell processes as Jurkat-CD48TM T-cells treated with sodium azide formed close contacts from which CD45 was excluded

bioRxiv preprint doi: https://doi.org/10.1101/109785; this version posted February 19, 2017. The copyright holder for this preprint (which was not certified by peer review) is the author/funder. All rights reserved. No reuse allowed without permission.

(**Figure S3C**). Furthermore, for Jurkat-CD48TM T-cells interacting with SLBs loaded with equal amounts of fluorescently-labeled CD45RABC and rCD2, CD45 was readily excluded from each contact, further confirming that CD45 segregation occurs passively (**Figure S3D** and **Movie S3**). Overall, the Lck/TCR ratio, which was ~2.7 prior to contact (based on 40,000 Lck molecules/cell), increased to 5.4 and 3.3 upon contact with the IgG-coated glass surfaces and SLBs, respectively. In contrast, the CD45/TCR ratio dropped from 13.3 prior to contact to 6.5-6.8 inside the close contacts. These effects would each be expected to favor TCR phosphorylation.

T-cell signaling dynamics following close contact formation

Having characterized the organization of close contacts, we next sought to explore the relationship between their spatiotemporal dynamics and T-cell signaling. To do so, we used interference reflection microscopy (IRM) to identify the areas of the close contact on IgG-coated surfaces, coupled with the simultaneous detection of cytoplasmic Ca^{2+} reporter (Fluo-4; **Figure 2A** and **Figure S4** and **Movie S4**). At the time of Ca^{2+} release, cells formed a median total contact area of 19 μm^2 (**Figure 2C**, *upper panel*). For cells interacting with SLBs, TIRF was used to simultaneously measure CD45 distribution and Fluo-4 fluorescence intensity (**Figure 2B** and **Movies S5, S6**). In this case signaling was detected as cells reached a median contact area of 6 μm^2 (**Figure 2C**, *lower panel*). The median delays between initial contact and signaling for the IgG-coated glass and SLB were 121 s and 146 s, respectively (**Figure 2D**). Using the median area reached at the time of signaling, we estimate that ~34 TCRs on IgG coated surfaces and ~86 TCRs on the SLBs were inside each close contact at the time signaling was detected, assuming a cell diameter of 11.5 μm and 15,000 TCR/cell (**Figure S5B**). Ligand-induced signaling has been shown to require fewer than 10 pMHCs and less than one minute (Irvine et al., 2002; O'Donoghue et al., 2013). Receptor triggering in the absence of ligands seems to rely on more TCRs and relatively large, stable contacts but otherwise readily occurs in our experiments. This implies that ligand-independent triggering must be actively constrained *in vivo*.

A new theoretical treatment of TCR signaling

Its ability to be triggered ligand-independently seemed at odds with the requirement that the TCR discriminate between ligands of differing quality. We investigated the extent to which these apparently contradictory features of TCR signaling could be reconciled by a theory of signaling contingent only upon TCR occupancy of close contacts. The model incorporated the following observables and parameters: (1) changes in CD45/Lck ratio, (2) TCR density and diffusion inside regions of close contact, and (3) the size and duration of close contacts. For circular close contacts, the mean dwell-time for a freely-diffusing TCR inside the contacts (τ_m) is dependent on their radius *r* and inversely proportional to the diffusion coefficient *D* of the TCR (**Figure 3A**):

$$\tau_m = r^2/8D$$

We assume that receptor triggering (CD3 ITAM phosphorylation) occurs if a single TCR remains inside the close contact for at least 2 seconds ($\tau = t_{min} = 2\,s$), based on the finding that TCR triggering occurs

bioRxiv preprint doi: https://doi.org/10.1101/109785; this version posted February 19, 2017. The copyright holder for this preprint (which was not certified by peer review) is the author/funder. All rights reserved. No reuse allowed without permission.

within two seconds of pMHC binding (Feinerman et al., 2008; Huse et al., 2007; Palmer and Naeher, 2009; Williams et al., 1999) and on our estimation of the effective Lck activity inside close contacts (close to 2.2 pTyr/s; see Hui and Vale, 2014 for the CD45/Lck ratio measured, *i.e.* 2 to 2.5). Since it is known that single ligands can trigger signaling in T cells (Irvine et al., 2002), and since TCRs will enter close contacts from their edges, a simple model based on mean dwell-time might not capture the actual distribution and contribution of individual receptors to signaling. We therefore developed a formal treatment of the evolution of TCR distribution and dwell-times in close contacts using partial differential equations and an equation describing TCR entrance rate (Weaver, 1983).

Using this model we calculated the dwell-times of individual TCRs and determined the probability p that any given receptor resides within a close contact for a dwell-time $\tau > 2\,s$, for contacts of various radii r (assuming a radius-dependent rate of entrance of TCRs into the contacts, **Movie S7**; see **Supplementary Information** for a full mathematical description; **Model 1**). The model predicts that the likelihood a TCR remains for longer than 2 s inside a close contact increases sharply with close contact radius (**Figure 3B**; see **Table S3** for all parameter values used) and that p is >0.1 for fixed-size close contacts of the size we observed at the time of signaling when T cells contact IgG-coated glass or SLBs (**Figure 2**). Given this probability, the overall TCR density (**Figure S5B**), and the level of TCR exclusion from the contacts (*i.e.* 60-95%, see **Figure 1H**), we calculated the number of triggered TCRs to be ~6 and ~16 on IgG-glass and the SLBs, respectively (**Figure 3C**). However, since close contacts were observed to grow in our experiments, we also calculated the triggering probability for contacts that grow to radius r by incorporating a novel moving-boundary analysis. In this case, TCR triggering probability increases sharply in the absence of ligands when close contacts reach ~0.2 μm radius, in agreement with the findings of Chang et al. (2016; **Figure 3D**; see **Table S3** for all parameter values used). For close contacts persisting for 120 to 180 seconds, the dependence of triggering probability on contact size was very similar (**Figure S5A**), indicating that for the timescales during which ligand-independent signaling is observed on these surfaces (**Figure 2**), triggering probability is not affected by contact duration.

It is noteworthy that a simpler treatment of the problem, which assumes a random, uniform distribution of TCRs inside the close contact and uses ordinary differential equations facilitating calculations, also shows that the probability of a TCR being triggered increases with close contact area (**Figure S6,** see **Supplementary Information** for a full mathematical description of the model; **Model 2**). Importantly, for both models TCR dwell-time is the sole parameter underpinning signaling; the models differ only in their assumptions and in their treatment of TCR density and distribution as close contacts grow.

Validation of the model

Since the residence time of a TCR in the close contact depends on the radius of the contact, growth of close contacts on time scales similar to or faster than TCR diffusion would be expected to induce faster

bioRxiv preprint doi: https://doi.org/10.1101/109785; this version posted February 19, 2017. The copyright holder for this preprint (which was not certified by peer review) is the author/funder. All rights reserved. No reuse allowed without permission.

receptor triggering (*i.e.* triggering after a shorter lag; **Figure 3E** and **Figure S5C**; see **Supplementary Information** for further details). Similar predictions are made by Model 2 (see **Figure S6C**). The triggering time is also directly related to t_{min}, the minimum time a TCR must remain within the close contact to be phosphorylated. We assumed t_{min} to be 2 seconds, based on *in vitro* measurements of Lck k_{cat} at a CD45/Lck ratio of ~2.3:1 (Hui and Vale, 2014), the ratio measured at close contacts. For comparison, if the k_{cat} of Lck were 10-fold lower (*e.g.* due to a higher CD45/Lck ratio), t_{min} would increase to 20s, reducing the likelihood of signaling and shifting the curve to longer triggering times (**Figure 3E;** blue line). Since close contact growth-rates and triggering time are parameters that are experimentally accessible, we could use the relationship between them to test two predictions of the new model: (1) that triggering is delayed for lower levels of CD45 segregation; and (2) that close contact growth-rate and the time taken for a cell to trigger are inversely correlated.

To test the first prediction, we compared the triggering times of Jurkat T-cells and cells expressing a form of CD45 (HA-CD45) lacking its extracellular domain, which is excluded from close contacts less efficiently than wild-type CD45 (**Figure S1A**). Expression of HA-CD45 at 5% of the total CD45 (*i.e.* ~10,000 copies/cell; **Figure S5E**) delayed triggering by almost 20 seconds ($p < 0.05$, two-tailed t test; **Figure 3F**). To test the second prediction, we simultaneously measured close contact growth-rates and signaling times. Both for contacts formed on IgG-coated glass and rCD2-SLBs, faster triggering was observed in cells with faster close contact growth-rates in good agreement with the predicted inverse relationship between close contact growth rate and the lag time preceding signaling (**Figure 3G** and **Figure S5D**). These observations indicate (1) that TCR triggering is indeed dependent on TCR dwell-time at close contacts, and (2) that the mean residence time, corresponding to a certain close contact area (Eq. 1), must exceed a threshold for triggering to occur (**Figure S5D**).

Close contact topography underpins signaling outcome

The foregoing analysis shows why receptor triggering is uncoupled from ligand binding if the cell forms stable and/or large enough close contacts depleted of CD45. Questions that arise are: how do T cells prevent ligand-independent TCR triggering *in vivo*, and what ensures the antigen specificity of responses? Our results indicate that T-cell signaling is sensitive to contact area and contact duration. Springer and co-workers measured T cell/APC contacts diameters of 0.43 ± 0.04 μm using TEM (Sage et al., 2012), and other work shows that T cell/APC contacts are brief, lasting between 1-5 minutes (Deguine et al., 2010; Ritter et al., 2015; Stoll et al., 2002). We therefore used our model to explore the extent to which signaling specificity might depend on close contact area and duration.

In the absence of ligands and for close contacts with a fixed r of 0.22 μm, the model predicted that it would take ~18 hours to achieve a 50% probability that any given TCR is triggered (**Figure 4A** and **Supplementary Information**), implying that ligand-independent triggering is highly unlikely for close contacts of the size reported by Sage *et al.* (2012). Strikingly, however, a 2-fold change in close contact radius yielded a ~1,000-fold increase in the probability of TCR triggering in the absence of

bioRxiv preprint doi: https://doi.org/10.1101/109785; this version posted February 19, 2017. The copyright holder for this preprint (which was not certified by peer review) is the author/funder. All rights reserved. No reuse allowed without permission.

ligands, resulting in 50% signaling likelihood being reached in just 70 s (**Figure 4A**). These observations suggest that close contact growth needs to be constrained *in vivo* to prevent unspecific T-cell activation.

To explore the extent to which ligands might further reduce the time required to reach 50% signaling probability *via* effects on TCR dwell-time at close contacts, we extended the model by incorporating the k_{on} and k_{off} (life-time, 1/ k_{off}) of TCR/pMHC interactions (**Supplementary Information**). Assuming low levels of agonist pMHC (30 pMHC/μm^2) and a contact radius of 0.22 µm, agonist pMHC binding (k_{off} = 1 s; k_{on} = 0.1 $\mu m^2 s^{-1}$) drastically reduced the time taken to reach 50% likelihood of signaling ~12,000-fold, *i.e.* from 18 hours to 5 seconds (close to t_{min}; **Figure 4B**). For pMHC/TCR interactions with k_{off} = 50 s^{-1} and for pMHC at 300 molecules/μm^2, *i.e.* at the observed lower-affinity threshold for agonistic TCR-pMHC interactions (Huang et al., 2010; Huppa et al., 2010; Krogsgaard et al., 2005; Morris and Allen, 2012), TCR signaling required the formation of stable contacts lasting 2.5 hours (**Figure 4B**), which is unlikely given the short-lived nature of T-cell/APC interactions (Deguine et al., 2010; Ritter et al., 2015; Stoll et al., 2002). Moreover, as expected, changes to both k_{on} or k_{off} altered the triggering probability profoundly (**Figure 4C**). Importantly, the model discriminated between known agonists and non-agonists using reported 2D pMHC/TCR interaction kinetics (**Figure 4D**; Huang et al. 2011). Similar results were obtained with Model 2 (**Figure S7**).

A final implication of the modeling is that, whereas ligand-independent TCR signaling was markedly dependent on close contact radius, agonist signaling was less so (**Figure 4E**), which profoundly skews their contributions to signaling as contact size varies. For close contacts smaller than 0.25 µm radius, the model predicts that pMHC agonists are the main drivers of TCR signaling (**Figure 4F**, *violet, orange, red* and *green traces*) whereas, for contacts larger than 0.25 µm radius, signaling readily occurs in the absence of ligand engagement (**Figure 4F**, **Figure S8;** *blue traces*). Therefore, the combination of pMHC/TCR affinity and close-contact size determines the number of triggered TCRs, and the ratio that are triggered ligand-dependently and –independently (**Figure 4F**, *insert*). Using the parameters in **Supplementary Table S4** and Model 2, it can be calculated that, for a contact of radius 0.8 µm, 27 TCRs sample 20 pMHCs on average, leading to 10 of the TCRs initiating signaling but only three of these being triggered ligand-dependently (**Figure S8**). Following an episode of specific signaling, therefore, continued growth of the contact could conceivably start to initiate significant levels of ligand-independent TCR triggering, amplifying incipient signaling.

The glycocalyx constrains close contact formation

We previously suggested that the formation of small close-contacts might help to restrict T-cell responses to cognate ligands *in vivo* (Chang et al., 2016), suggestions now reinforced by our modelling. But what factors might determine close contacts size? All lymphoid cells express very large amounts of highly glycosylated proteins such as CD45 and CD43, forming the glycocalyx, but these proteins are rarely if ever included in model bilayer systems and so their impact on T-cell contact

bioRxiv preprint doi: https://doi.org/10.1101/109785; this version posted February 19, 2017. The copyright holder for this preprint (which was not certified by peer review) is the author/funder. All rights reserved. No reuse allowed without permission.

formation is unclear. We studied the interaction of T cells with surfaces containing CD45 to mimic the glycocalyx and CD2 to favor adhesion. In the absence of CD45, large fractions of Jurkat T-cells contacting Ni-NTA-coated, histidine-tagged CD2-presenting glass surfaces released Ca^{2+} and formed frequent and stable attachments to the surface (**Figure 5A**). Addition of histidine-tagged CD45RABC at a CD2/CD45RABC ratio of 1:15 reduced the fractions of triggered cells more than three-fold and attached cells more than four-fold (**Figure 5A** and **D**). Similarly, incorporation of CD45RABC into SLBs co-presenting physiological levels of CD2 (200-300 molecules/μm^2) reduced the numbers of contact-forming cells more than 5-fold (**Figure 5B**-**D**; **Supplementary Figure 9** and **Movie S8**) and reduced signaling 40-fold (**Figure 5B**-**D**). On the rare occasions close contact formation was observed, the SLB-bound CD45 was excluded from the contacts and around 75% of these cells produced calcium responses (**Movie S9**), indicating that the presence of CD45 on model surfaces prevents TCR triggering by inhibiting close contact formation in the first place. These observations suggest that the glycocalyx likely comprises a substantial barrier to ligand-independent TCR triggering *in vivo*.

Discussion

Here, we sought the reasons why TCR signaling can be ligand-specific without the triggering mechanism being strictly ligand-dependent (Chang et al., 2016). We characterized the diffusion of signaling proteins at close contacts on model surfaces lacking TCR ligands, and then developed a theoretical treatment of receptor triggering that reveals how signaling is likely to be influenced by the spatiotemporal properties of contact formation.

TIRF imaging showed that close contacts are dynamic structures with small, multifocal, initially-formed contacts merging into single, larger ones over time. Super-resolution imaging implied that close contacts form spontaneously and passively since CD45 was excluded from contacts as small as ~80 nm. Tracking the TCR, CD45 and Lck revealed that IgG-coated glass surfaces induce the exclusion (>80%) of all proteins with extracellular domains. Intriguingly, two-thirds of Lck molecules were also excluded from close contacts, implying that the "barrier" extends across the cell membrane. Possible explanations for this are that crowding effects operate at the contact boundary, or that a diffusional barrier is created by interactions between CD45 and the cytoskeleton following receptor signaling (Freeman et al., 2016). On SLBs, which more closely mimic the close contacts expected to form *in vivo*, the overall extent of CD45, Lck and TCR segregation was lower, with CD45 being most affected (also >80% excluded). However, the Lck/CD45 ratio increased only ~2-fold inside the contacts formed on both model surfaces, and for SLBs there were similar small increases in Lck/TCR (3 fold) and TCR/CD45 (6 fold) ratio. Overall, relatively modest changes in TCR/Lck/CD45 equilibrium seem therefore to be capable of initiating signaling in T cells, explaining the dramatic effects of *e.g.* pharmacological interventions (O'Shea et al., 1992). TCR diffusion was ~2-fold slower compared to CD45 and Lck, but unchanged in close contacts formed on SLBs, indicating that close contact formation will only ever enhance TCR scanning of APCs for antigen. Larger median areas of contact were required for signaling to be initiated on IgG-coated glass than on SLBs (19 μm^2 versus 6 μm^2),

bioRxiv preprint doi: https://doi.org/10.1101/109785; this version posted February 19, 2017. The copyright holder for this preprint (which was not certified by peer review) is the author/funder. All rights reserved. No reuse allowed without permission.

likely reflecting differences in TCR densities (and thus numbers present) in the close contacts (~34 and 86 TCRs, respectively).

Our new theoretical treatment of signaling, which depends only on TCR dwell-time at close contacts, accounts for both ligand discrimination and sensitivity. The model used measurements of (1) changes in CD45/Lck ratio at close contacts; (2) TCR density and diffusion; (3) the size and duration of close contacts; and (4) estimates of Lck activity expected at the CD45 and Lck segregation levels observed (Hui and Vale, 2014). Based on these parameters, we modeled the evolution of TCR density (and therefore dwell-time) in close contacts, using either moving-boundary passage time calculations accounting for the effect of contact growth and initial TCR position on the probability of TCR escape from the close contact, or a second approach that simply assumes an even distribution of TCRs across the contact and thus greatly facilitates calculations. Both approaches gave similar results, suggesting that the predictions of the model are robust with respect to the exact treatment of TCR distribution and flux. We validated the model by showing that in the absence of TCR ligands signaling was delayed when there was less CD45 segregation and that the rate of close contact growth and triggering time were inversely correlated. The model suggested that the probability of ligand-independent TCR triggering increases sharply for close contacts of radius ~0.2 μm. For close contacts formed on IgG-coated glass and SLBs in our experiments, we estimated that ~30-80 TCRs would be present at the time of signaling and that ~20% of these would be triggered (*i.e.* spend >2 s in close contacts), despite the absence of ligands. A similar number of TCRs have to be engaged by conventional ligands in order to observe T-cell signaling when $CD4^+$ T-cells interact with APCs in the absence of co-receptor engagement (~30 TCRs; Irvine et al., 2002). Overall, our observations suggest that TCR triggering could be so simple as to depend only on receptor occupancy of close contacts, with mean residence time having only to exceed a threshold for triggering to occur. Based on this, we propose that pMHC specific responses are governed by the thermodynamics of TCR/pMHC interactions (Boniface et al., 1999; Willcox et al., 1999; Wu et al., 2002) along with TCR diffusion rate, CD45 exclusion efficiency and T-cell topography, as all of these components influence mean residence time.

We used the model to ask how T cells avoid ligand-independent TCR triggering *in vivo*, and how the TCR discriminates between different-quality ligands. In the absence of ligands and for close contacts of the size observed *in vivo*, *i.e.* r=0.22 μm, our model suggests that it would take several days to trigger just one TCR, implying that ligand-independent triggering, although readily observable *in vitro*, is unlikely to generate unwanted signaling *in vivo*. A very surprising outcome was the remarkable sensitivity of ligand-independent signaling to close contact area, however: an increase in contact radius of only 2-fold produced a three orders-of-magnitude increase in the probability of signaling, making it likely to occur within 70s. The size of close contacts observed *in vivo* therefore seems to be close to the threshold needed for ligand-independent TCR signaling. The dependence of triggering probability on the radius is sigmoidal, suggesting that signaling could be subject to switch-like behavior. These findings have several interesting implications. First, the size of close contacts

bioRxiv preprint doi: https://doi.org/10.1101/109785; this version posted February 19, 2017. The copyright holder for this preprint (which was not certified by peer review) is the author/funder. All rights reserved. No reuse allowed without permission.

committing T-cells to synapse formation might be tightly controlled so that non-specific activation is avoided. Second, for close contacts increasing beyond the threshold favoring ligand-specific responses and following, perhaps, an initial round of receptor triggering, ligand-independent triggering could act to reinforce or amplify signaling by increasing the number of triggered receptors beyond those engaged by ligands. Third, defects in cellular processes constraining close contacts size could predispose to autoimmunity by increasing non-specific (ligand-independent) receptor triggering.

The new model also explains why pMHC ligands so profoundly alter the likelihood of signaling and accounts for ligand discrimination. For TCRs interacting with typical ligands in a 0.22 μm radius close contact, agonist-dependent versus -independent signaling is favored as much as 12,000-fold. On the other hand, ligands modelled at 300 molecules/μm^2 and with k_{off} 50 s^{-1}, *i.e.* weak agonists or potent "self" ligands, take minutes rather than seconds to initiate signaling, allowing robust discrimination. Accordingly, we could distinguish between authentic agonists and non-agonists with known 2D pMHC/TCR interaction kinetics (Huang et al. 2011) using the new model. Previously, kinetic proof-reading (KP) schemes have been used to explain ligand discrimination, with k_{off} determining the extent of downstream processing of signaling complexes needed to distinguish between ligands (McKeithan, 1995; Burroughs et al., 2006). Ligand discrimination was proposed to require multiple, reversible intermediate steps, in contrast to "conventional" receptors such as GPCRs triggered in a binary fashion (McKeithan, 1995). The 2 s triggering threshold assumed in our model reflects the rate at which Lck phosphorylates the TCR (Hui and Vale, 2014). Our model therefore suggests that TCR phosphorylation alone allows robust discrimination between ligands. Previously, in stochastic simulations of the KS model, multiple proofreading steps and longer delays were required because kinase activity was assumed to be increased 200-fold inside versus outside close contacts (Burroughs et al. 2006). Our data indicate that relatively modest increases in net kinase activity accompany close contact formation, reducing the likelihood that weakly bound receptors are phosphorylated. If, as our data suggest, triggering depends on TCR dwell time at CD45-depleted close-contacts, discrimination will rely not only on k_{off} but also on k_{on} and ligand concentration. This may explain previous reports that both k_{on} and k_{off} can critically influence signaling outcome (Aleksic et al. 2010; Huang et al. 2010; Huppa et al. 2010). Given the importance of the size of the initial close contact formed, the size and the topography of the structures T-cells could use to probe target cells, i.e. microvilli (Jung et al. 2016) may have had some role in the evolution of a ligand discriminating mechanism.

Finally, our results indicate that any general property of the lymphocyte cell surface that impacts on the formation of close contacts will likely have a large bearing on T-cell responsiveness. A particularly noteworthy example is CD45 itself, which when placed on our model surfaces to mimic the glycocalyx present on professional APCs, profoundly blocked close contact formation and T-cell signaling in the absence of antigen but in the presence of small adhesion molecules. In this way CD45 might act as a major barrier to non-specific activation during T-cell priming *in vivo*. The challenge now is to understand whether T cells form close contacts while forming authentic cell-cell conjugates, and if so,

bioRxiv preprint doi: https://doi.org/10.1101/109785; this version posted February 19, 2017. The copyright holder for this preprint (which was not certified by peer review) is the author/funder. All rights reserved. No reuse allowed without permission.

how barriers to their formation such as the glycocalyx are overcome. In conclusion, our work offers new insights into the molecular basis of the initiation of T-cell responses and provides a new quantitative framework for making predictions that can be tested in future studies of TCR triggering.

Acknowledgements

This work was funded by The Wellcome Trust, the UK Medical Research Council, the UK Biotechnology and Biological Sciences Research Council and Cancer Research UK. We thank the Wolfson Imaging Centre, University of Oxford, for access to the microscope facility. We would like to thank the Wellcome Trust for the Sir Henry Dale Fellowship of RAF (WT101609MA). We would like to thank the Royal Society for the University Research Fellowship of SFL (UF120277) and acknowledge a GSK Professorship (DK).

Author contributions

R.A.F. and K.A.G. designed and performed experiments, analyzed data and R.A.F, K.A.G, S.J.D and D.K. wrote the manuscript with input from all authors. J.T., A.E.L, O.D. and A.T., designed all mathematical modelling. P.J., S.F.L. and M.P performed TIRF experiments and super-resolution microscopy. V.T.C expressed and purified soluble CD45. A.M.S. performed calcium experiments and IRM. B.C.M designed the IRM setup. C.M. performed single molecule tracking experiments under supervision of K.A.G. S.J.D. and D.K. conceived and supervised the project.

References

Altan-Bonnet, G., and Germain, R.N. (2005). Modeling T Cell Antigen Discrimination Based on Feedback Control of Digital ERK Responses. PLoS Biol. *3*, e356.

Burroughs, N.J., Lazic, Z., and van der Merwe, P.A. (2006). Ligand detection and discrimination by spatial relocalization: A kinase-phosphatase segregation model of TCR activation. Biophys. J. *91*, 1619–1629.

Chakraborty, A.K., and Weiss, A. (2014). Insights into the initiation of TCR signaling. Nat. Immunol. *15*, 798–807.

Chui, D., Ong, C.J., Johnson, P., Teh, H.S., and Marth, J.D. (1994). Specific CD45 isoforms differentially regulate T cell receptor signaling. EMBO J. *13*, 798–807.

Dushek, O., and van der Merwe, P.A. (2014). An induced rebinding model of antigen discrimination. Trends Immunol. *35*, 153–158.

Dushek, O., van der Merwe, P.A., and Shahrezaei, V. (2011). Ultrasensitivity in multisite phosphorylation of membrane-anchored proteins. Biophys. J. *100*, 1189–1197.

Evans, E.J., Castro, A.A., Brien, R.O., Kearney, A., Walsh, H., Sparks, L.M., Tucknott, M.G., Davies, E.A., Carmo, A.M., Merwe, P.A. Van Der, et al. (2006). Crystal Structure and Binding Properties of the CD2. J. Biol. Chem. *281*, 29309–29320.

Feinerman, O., Veiga, J., Dorfman, J.R., Germain, R.N., and Altan-Bonnet, G. (2008). Variability and robustness in T cell activation from regulated heterogeneity in protein levels. Science *321*, 1081–1084.

Garcia, K.C., Scott, C.A., Brunmark, A., Carbone, F.R., Peterson, P.A., Wilson, I.A., and Teyton, L. (1996). CD8 enhances formation of stable T-cell receptor/MHC class I molecule complexes. Nature

bioRxiv preprint doi: https://doi.org/10.1101/109785; this version posted February 19, 2017. The copyright holder for this preprint (which was not certified by peer review) is the author/funder. All rights reserved. No reuse allowed without permission.

384, 577–581.

George, A.J.T., Stark, J., and Chan, C. (2005). Understanding specificity and sensitivity of T-cell recognition. Trends Immunol. *26*, 653–659.

Groves, J.T., and Dustin, M.L. (2003). Supported planar bilayers in studies on immune cell adhesion and communication. J. Immunol. Methods *278*, 19–32.

Huang, J., Zarnitsyna, V.I., Liu, B., Edwards, L.J., Jiang, N., Evavold, B.D., and Zhu, C. (2010). The kinetics of two-dimensional TCR and pMHC interactions determine T-cell responsiveness. Nature *464*, 932–936.

Hui, E., and Vale, R.D. (2014). In vitro membrane reconstitution of the T-cell receptor proximal signaling network. Nat. Struct. Mol. Biol. *21*, 133–142.

Huppa, J.B., Axmann, M., Mörtelmaier, M.A., Lillemeier, B.F., Newell, E.W., Brameshuber, M., Klein, L.O., Schütz, G.J., and Davis, M.M. (2010). TCR-peptide-MHC interactions in situ show accelerated kinetics and increased affinity. Nature *463*, 963–967.

Huse, M., Klein, L.O., Girvin, A.T., Faraj, J.M., Li, Q.-J., Kuhns, M.S., and Davis, M.M. (2007). Spatial and temporal dynamics of T cell receptor signaling with a photoactivatable agonist. Immunity *27*, 76–88.

Irvine, D.J., Purbhoo, M. a, Krogsgaard, M., and Davis, M.M. (2002). Direct observation of ligand recognition by T cells. Nature *419*, 845–849.

Jönsson, P., Southcombe, J.H., Santos, A.M., Huo, J., Fernandes, R.A., McColl, J., Lever, M., Evans, E.J., Hudson, A., Chang, V.T., et al. (2016). Remarkably low affinity of CD4/peptide-major histocompatibility complex class II protein interactions. Proc. Natl. Acad. Sci. U. S. A. *113*, 5682–5687.

Jung Y, Riven I, Feigelson SW, Kartvelishvily E, Tohya K, Miyasaka M, Alon R, Haran G. (2016). Three-dimensional localization of T-cell receptors in relation to microvilli using a combination of superresolution microscopies. Proc Natl Acad Sci U S A. *113*, 5916-5924.

Kim, P.W., Sun, Z.-Y.J., Blacklow, S.C., Wagner, G., and Eck, M.J. (2003). A zinc clasp structure tethers Lck to T cell coreceptors CD4 and CD8. Science *301*, 1725–1728.

Ma, Z., Janmey, P.A., and Finkel, T.H. (2008). The receptor deformation model of TCR triggering. FASEB J. *22*, 1002–1008.

Manjunath, N., Correa, M., Ardman, M., and Ardman, B. (1995). Negative regulation of T-cell adhesion and activation by CD43. Nature *377*, 535–538.

van der Merwe, P.A., and Dushek, O. (2011). Mechanisms for T cell receptor triggering. Nat. Rev. Immunol. *11*, 47–55.

Morris, G.P., and Allen, P.M. (2012). How the TCR balances sensitivity and specificity for the recognition of self and pathogens. Nat. Immunol. *13*, 121–128.

Novak, T.J., Farber, D., Leitenberg, D., Hong, S., Johnson, P., and Bottomly, K. (1994). Isoforms of the transmembrane tyrosine phosphatase cd45 differentially affect T cell recognition. Immunity *1*, 109–119.

O'Donoghue, G.P., Pielak, R.M., Smoligovets, A.A., Lin, J.J., and Groves, J.T. (2013). Direct single molecule measurement of TCR triggering by agonist pMHC in living primary T cells. Elife *2*, e00778.

Palmer, E., and Naeher, D. (2009). Affinity threshold for thymic selection through a T-cell receptor–co-receptor zipper. Nat. Rev. Immunol. *9*, 207–213.

Rabinowitz, J.D., Beeson, C., Lyons, D.S., Davis, M.M., and McConnell, H.M. (1996). Kinetic discrimination in T-cell activation. Proc. Natl. Acad. Sci. *93*, 1401–1405.

Sage, P.T., Varghese, L.M., Martinelli, R., Sciuto, T.E., Kamei, M., Dvorak, A.M., Springer, T.A., Sharpe, A.H., and Carman, C. V (2012). Antigen recognition is facilitated by invadosome-like

bioRxiv preprint doi: https://doi.org/10.1101/109785; this version posted February 19, 2017. The copyright holder for this preprint (which was not certified by peer review) is the author/funder. All rights reserved. No reuse allowed without permission.

protrusions formed by memory/effector T cells. J. Immunol. *188*, 3686–3699.

Smith-Garvin, J.E., Koretzky, G.A., and Jordan, M.S. (2009). T cell activation. Annu. Rev. Immunol. *27*, 591–619.

Trop, S., Charron, J., Arguin, C., Lesage, S., and Hugo, P. (2000). Thymic selection generates T cells expressing self-reactive TCRs in the absence of CD45. J. Immunol. *165*, 3073–3079.

Valitutti, S., Müller, S., Cella, M., Padovan, E., and Lanzavecchia, A. (1995). Serial triggering of many T-cell receptors by a few peptide-MHC complexes. Nature *375*, 148–151.

Williams, C.B., Engle, D.L., Kersh, G.J., Michael White, J., and Allen, P.M. (1999). A Kinetic Threshold between Negative and Positive Selection Based on the Longevity of the T Cell Receptor-Ligand Complex. J. Exp. Med. *189*, 1531–1544.

Yin, Y., Wang, X.X., and Mariuzza, R.A. (2012). Crystal structure of a complete ternary complex of T-cell receptor, peptide-MHC, and CD4. Proc. Natl. Acad. Sci. U. S. A. *109*, 5405–5410.

bioRxiv preprint doi: https://doi.org/10.1101/109785; this version posted February 19, 2017. The copyright holder for this preprint (which was not certified by peer review) is the author/funder. All rights reserved. No reuse allowed without permission.

bioRxiv preprint doi: https://doi.org/10.1101/109785; this version posted February 19, 2017. The copyright holder for this preprint (which was not certified by peer review) is the author/funder. All rights reserved. No reuse allowed without permission.

Figures

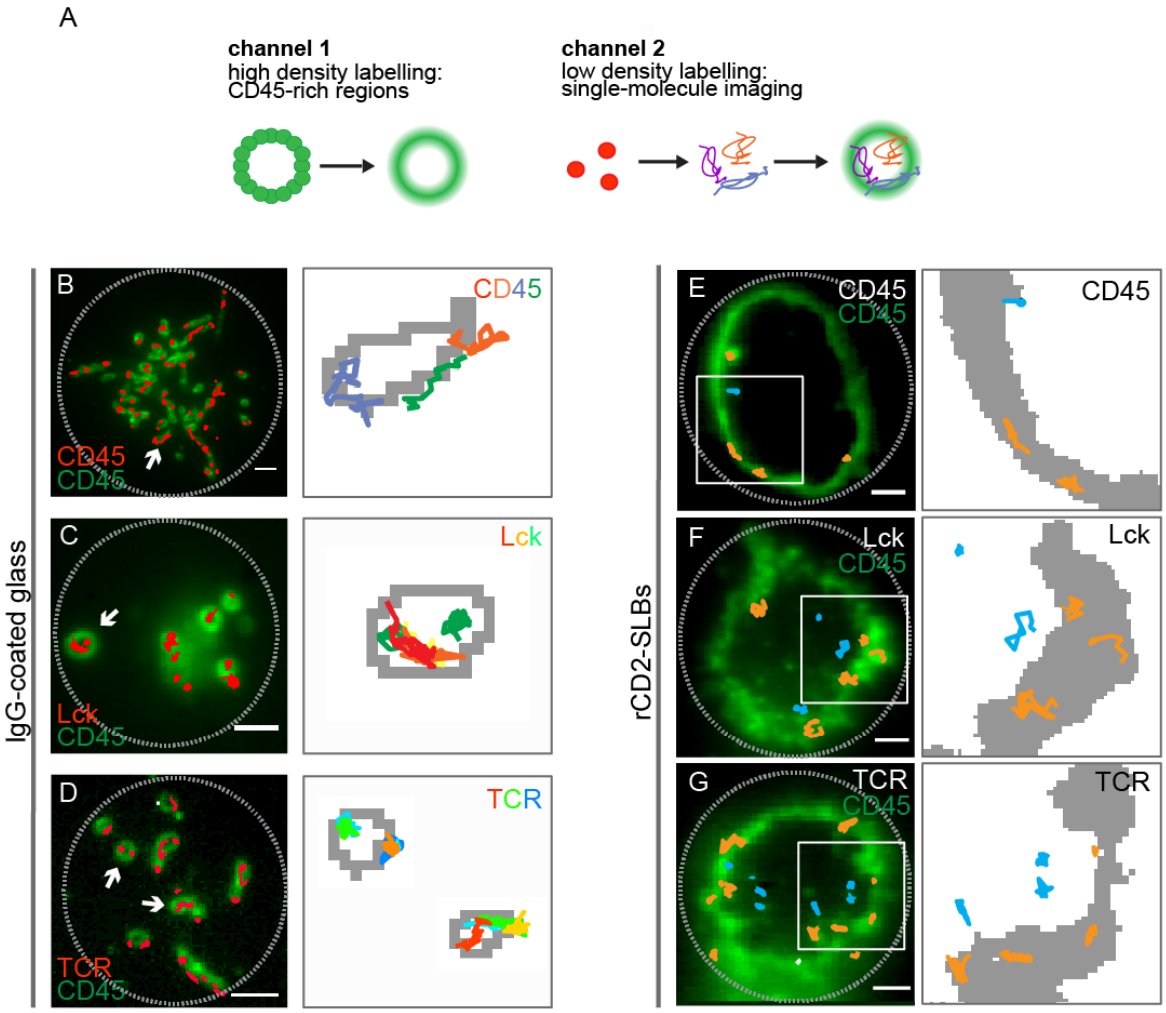

H

		Confined*/ total densities†	Diffusion Coefficient [μm²/s] "inside"	"outside"
IgG-coated glass	CD45	0.032±0.007		
	Lck (mm)	0.333±0.026		
	Lck (wt)	0.057±0.011		
	TCR-β	0.053±0.015	0.027±0.028	
	HA-CD45	0.138±0.018		
rCD2-SLBs	CD45	0.125±0.026		0.113±0.179
	Lck (wt)	0.556±0.067	0.151±0.294	0.104±0.185
	TCR-β	0.399±0.055	0.054±0.107	0.050±0.074

Measurable contacts are defined as spatially isolated zones of CD45 segregation that are larger than the diffraction limit.*Trajectories were classified a "confined" if they could be mapped exclusively onto the inner area of a zone (denoted wtih a gray boundary in the binary representation of the zones in panels b-h); †Quoted is the fraction of trajectory densities rather than numbers.

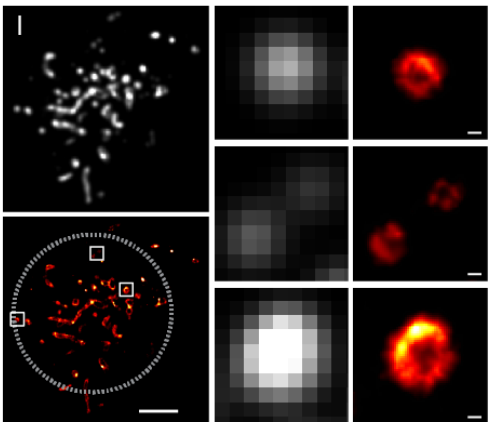

bioRxiv preprint doi: https://doi.org/10.1101/109785; this version posted February 19, 2017. The copyright holder for this preprint (which was not certified by peer review) is the author/funder. All rights reserved. No reuse allowed without permission.

Figure 1. Single-molecule analysis of CD45, Lck and TCR distribution at close-contacts formed between T cells and protein coated surfaces. (A) High-density labeling of CD45 was used to reveal sites of close contact formation (*left panel*) and combined with simultaneous low-density labeling of CD45, Lck or TCR (*right panel*) for TIRF-based single-molecule tracking. Trajectories of CD45 (**B**), Lck (**C**) and TCR (**D**) in close contacts marked by CD45 (*left column*; anti-CD45 Fab Alexa Fluor 488, *green*; single-molecule trajectories (yellow or red) over more than 280ms. All scale bars are 2 µm. *Right column*: magnified trajectories of CD45, Lck and TCR from CD45-rich areas (grey) for a single close contact as indicated by arrows in the *left* panels. (**E-G**) High-density labeling of CD45 (*green*, right panels) defines the edge of the close-contact formed between T cells and rat CD2 SLBs. TIRFM-based single-molecule tracking of CD45 (**E**), Lck (**F**) and TCR (**G**): well-separated individual trajectories were recorded over more than 280ms and colored according to relative position to CD45-rich areas (orange in CD45-rich area and blue in CD45 segregated area). *Right column*: zoom in on trajectories in areas marked by white rectangles; CD45-rich areas shown in grey. Scale bars are 2 µm. **(H)** Summary of parameters measured for molecules in close contacts formed on IgG or rat CD2 SLBs for which representative images are shown. (**I**) Super-resolution *d*STORM image of fluorescently labeled anti-CD45 Fab in early T cell contacts formed with IgG coated glass surface; average (*top left*) and reconstructed image (*bottom left,* scale bar 3 µm), demonstrating that CD45 is excluded from contacts as small as 78 nm in diameter. Zoom-in on three contacts (*right*, average and reconstructed images, scale bar 100 nm). Note that the CD45 distribution appears to be homogeneous across these contacts if the resolution is limited by diffraction.

bioRxiv preprint doi: https://doi.org/10.1101/109785; this version posted February 19, 2017. The copyright holder for this preprint (which was not certified by peer review) is the author/funder. All rights reserved. No reuse allowed without permission.

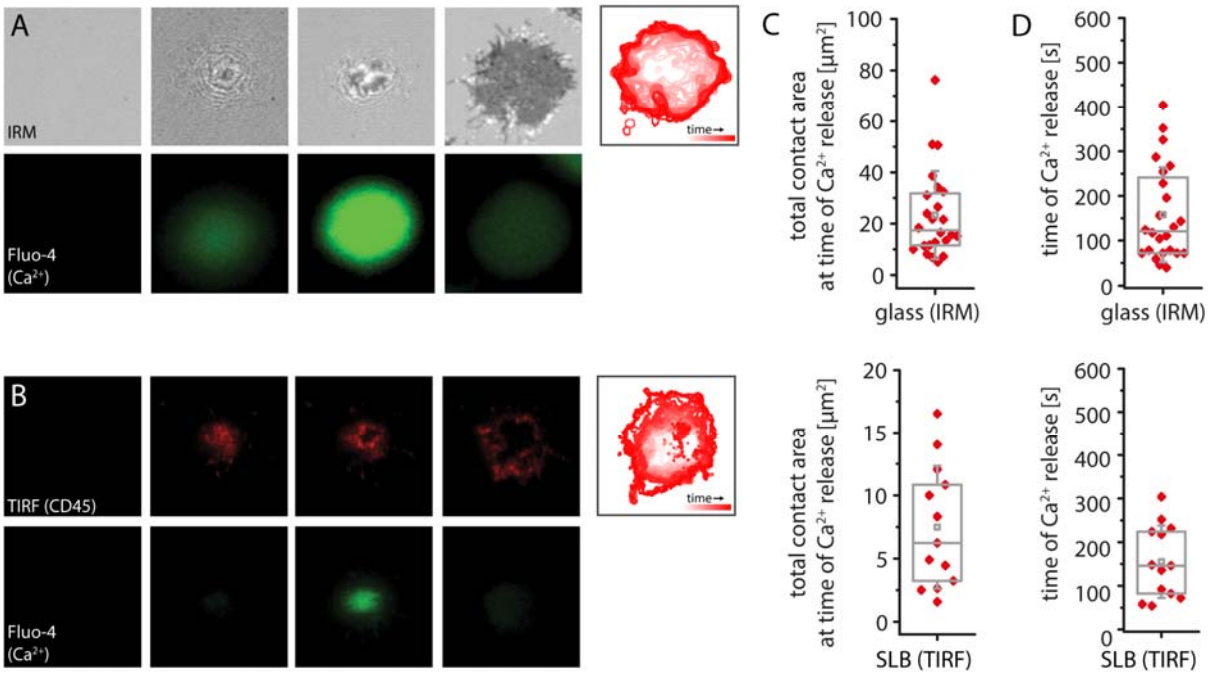

Figure 2. CD45 segregation is observed at sub-µm sized close-contacts formed between T cells and protein coated surfaces. (**A**, **B**) Time-resolved detection of close contact formation and simultaneous Ca^{2+} release measurement (Fluo-4, bottom panels) for cells landing on IgG coated glass using IRM (**A**; top panel; contour traces are shown for the smaller early contacts) or rCD2 SLBs (**B**; anti-CD45 Fab labeled with Alexa647, TIRFM; top panel). Corresponding temporal color-coded representation of the evolution of the close contact outer edge over time (corresponding *top right panel* in **A** and **B**; color-coded for time). (**C**) Total contact area at the time of calcium released for T cells interacting with IgG glass coated surfaces (*top panel*; 24 cells) or rCD2-SLBs (*bottom panel*; 13 cells). (**D**) Time of calcium released for T cells interacting with IgG glass coated surfaces (*top panel*; 24 cells) or rCD2-SLBs (*bottom panel*; 13 cells). For box plots in **C** and **D**, central lines indicate the median; small squares indicate the mean; boxes show interquartile range; whiskers are the s.d.

bioRxiv preprint doi: https://doi.org/10.1101/109785; this version posted February 19, 2017. The copyright holder for this preprint (which was not certified by peer review) is the author/funder. All rights reserved. No reuse allowed without permission.

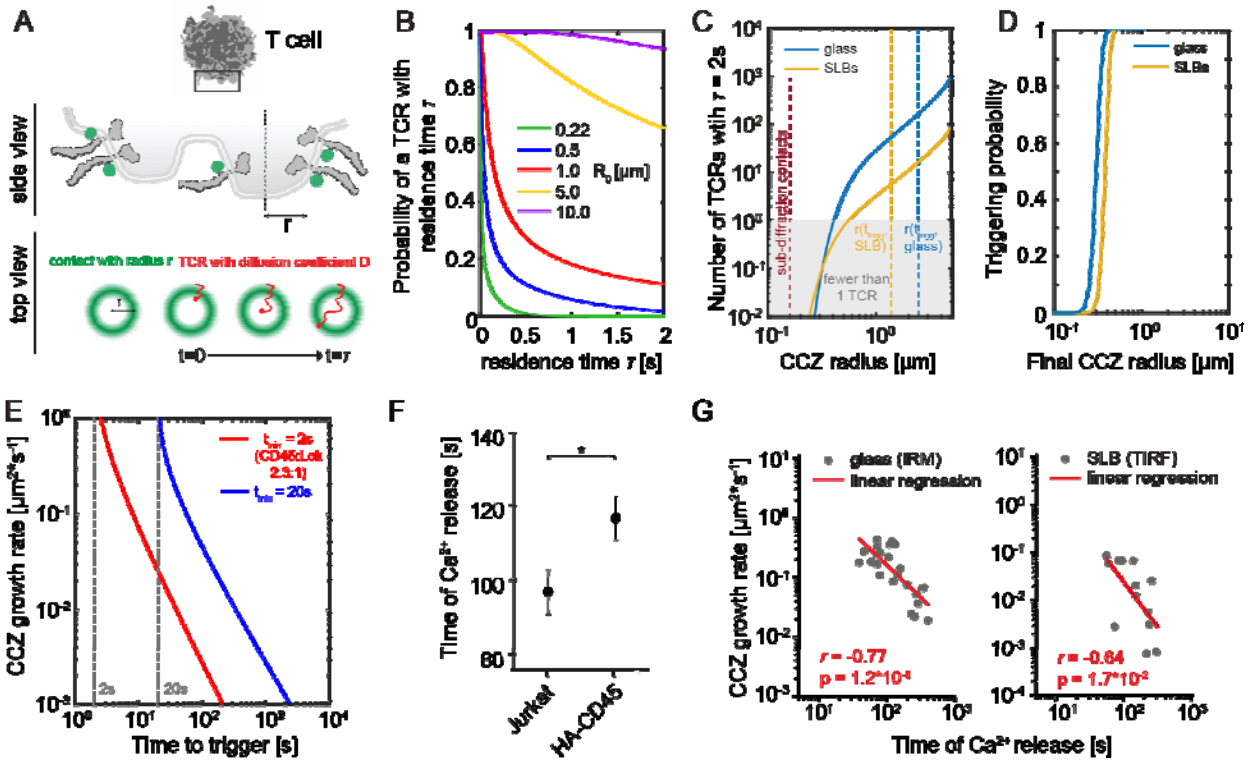

Figure 3. Analysis of ligand-independent TCR triggering dependence on close-contact zone area and duration. (**A**) Top- and side-view depiction of the components integrated in the mathematical modelling: segregation of CD45, contact topography (area and duration) and TCR mean residence time inside close contact. (**B**) Probability that a TCR remains inside a close contact for the time τ for close contacts of varying radius R_0 (all parameters can be found in **Tab. S3**). (**C**) Total number of TCRs that remain inside the close contact for longer than 2 seconds, taking into account the estimates shown in (**B**), the density of TCRs in Jurkat T cells and the segregation of TCR from close contacts for cells interacting with IgG-coated glass surfaces (blue line) or rCD2-SLBs (yellow line). (**D**) Probability that a single TCR stays inside a close contact > 2 s as a function of final close contact radius. (**E**) Time taken to TCR triggering as a function of growth rate of close contact zones. For a t_{min} = 20 (higher CD45:Lck ratio, blue line) triggering takes on average 10x longer at a given close contact growth rate *g* than for a CD45:Lck ratio of 2.3:1 (red line). (**F**) Quantification of the time delay between initial contact of cells with rCD2 SLBs and Ca^{2+} release for Jurkat T cells and Jurkat T cells expressing HA-CD45; p=0.02, two-tailed t-test, unequal variance assumed; errors are s.e.m. (**G**) The growth rate of close contact zones is inversely correlated with the time taken to triggering (large negative Pearson correlation coefficient *r* on logarithmic scale, values for *r* and *p* as indicated in the plot).

bioRxiv preprint doi: https://doi.org/10.1101/109785; this version posted February 19, 2017. The copyright holder for this preprint (which was not certified by peer review) is the author/funder. All rights reserved. No reuse allowed without permission.

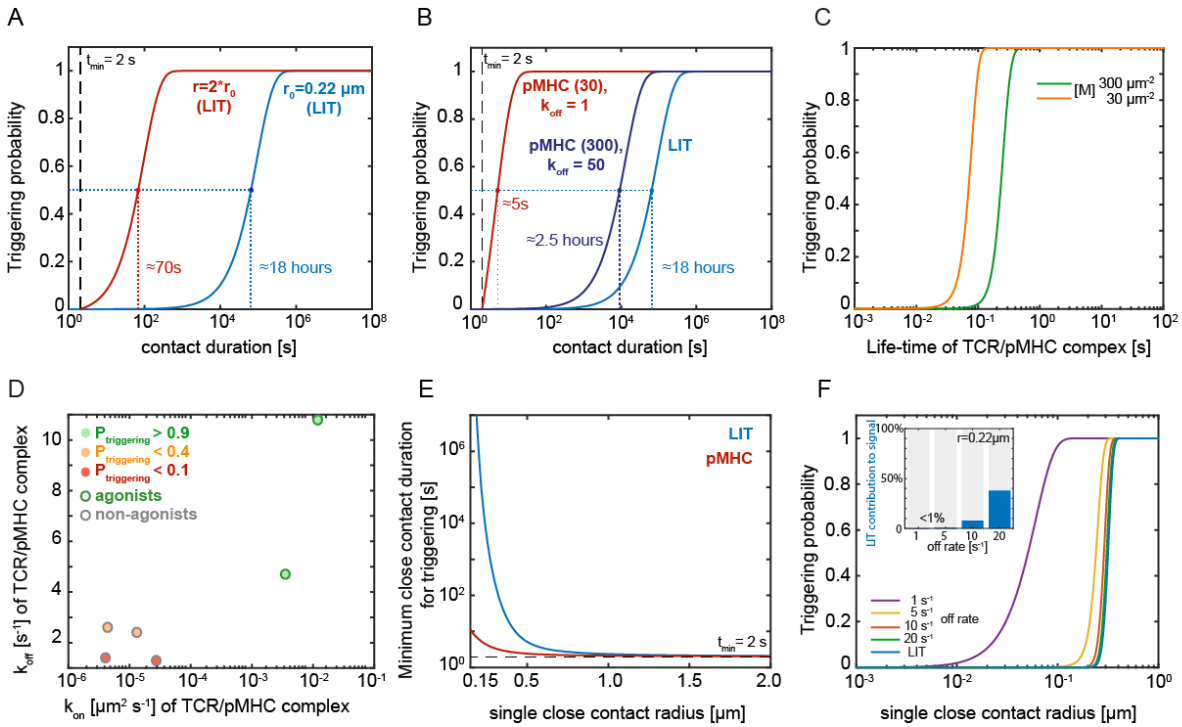

Figure 4. Analysis of TCR triggering dependency on ligand-binding and LIT contribution towards T cell activation. (**A**) Triggering probability of at least one TCR as function of contact duration in the absence of ligand. Triggering probability was determined for a single close contact of a 0.22 µm radius (as reported *in vivo* for close contacts formed between T cells and APCs) and for a larger close contact (0.44 µm; LIT, ligand independent TCR triggering). (**B**) Triggering probability of at least one TCR as a function of contact duration in the presence and absence of agonist pMHC with a low k_{off} (k_{off} = 1, 30 pMHC molecules/µm^2) and of a pMHC with a larger k_{off} at higher pMHC densities (k_{off} = 50, 300 pMHC molecules/µm^2) for a single close contact of 0.22 µm radius. (**C**) Triggering probability as a function of pMHC-TCR life-time ($1/k_{off}$) for different pMHC densities [M]. (**D**) Predicting T cell signalling using the mathematical model here derived for pMHC-TCR interactions (closed circle) with known 2D k_{on} and k_{off} affinities (Huang et al. 2010) and known to be T cell agonists or non-agonists (open circle); the color code indicates the probability that a single T cell triggering event (τ > 2 s) takes place when a contact persists for 120s (single contact of radius 0.22 µm; closed circle). (**E**) Effect of the close contact radius on the contact time required for T cell triggering in the presence or absence of agonist pMHC (k_{off} = 1, 30 pMHC molecules/µm^2). (**F**) Dependence of the triggering probability for TCRs on contact radius in the presence of agonist pMHC with varying k_{off} (30 pMHC molecules/µm^2) and in the absence of pMHCs (LIT; blue line). The insert shows the extent to which triggering results from TCRs which are triggered without binding to pMHC ('LIT').

bioRxiv preprint doi: https://doi.org/10.1101/109785; this version posted February 19, 2017. The copyright holder for this preprint (which was not certified by peer review) is the author/funder. All rights reserved. No reuse allowed without permission.

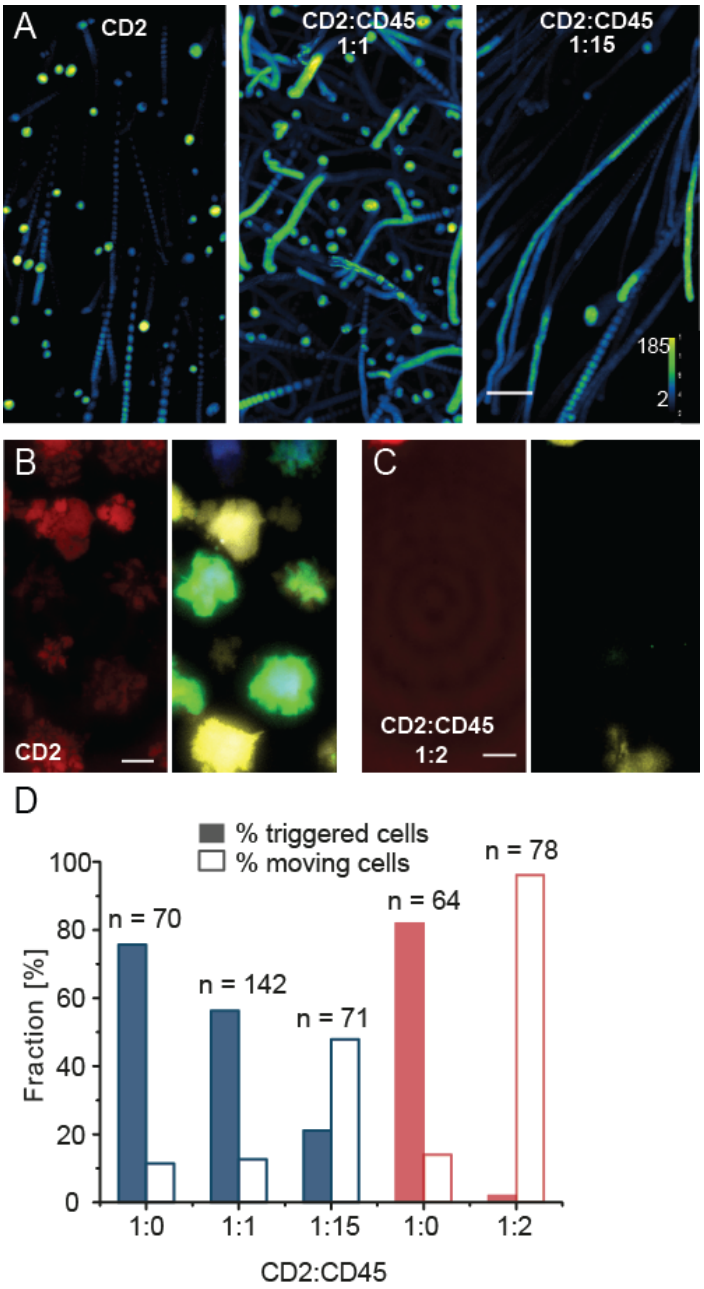

Figure 5. CD45 extracellular domain impairs close contact formation and reduces LIT. (**A**) Time lapse of intensity color-coded cells landing on nickel glass surface presenting rat CD2 (*left panel*), rat CD2 and CD45 at a 1 to 1 ratio (*middle panel*) or 1 to 15 ratio (*right panel*). Color traces indicate cell movement over acquisition times and bright colours (dark blue to yellow) indicate intensity of Ca^{2+} triggering. (**B**) Temporal projection (8 min) of rCD2 accumulation (*left panel*; rCD2 labeled with Alexa Fluor 647) and Ca^{2+} release (*right panel*) on bilayers displaying physiological levels of rCD2. (**C**) Adding hCD45RABC at a 2:1 ratio over physiological levels of rCD2 impairs accumulation of this adhesion protein in cell-SLB contacts (left panel; temporal projection) and no Ca^{2+} release was

bioRxiv preprint doi: https://doi.org/10.1101/109785; this version posted February 19, 2017. The copyright holder for this preprint (which was not certified by peer review) is the author/funder. All rights reserved. No reuse allowed without permission.

detected (right panel; temporal projection). (**D**) Quantification of the fraction of triggered cells and moving cells at different CD2:CD45 ratios on cells interacting with protein-coated glass (*blue*) or supported-lipid bilayers (*red*).

bioRxiv preprint doi: https://doi.org/10.1101/109785; this version posted February 19, 2017. The copyright holder for this preprint (which was not certified by peer review) is the author/funder. All rights reserved. No reuse allowed without permission.

Supplementary Information

Contents

I. STAR Methods

II. Supplementary Tables

Table S1 | Quantitative characterization of close contacts between T cells and glass surfaces and the organization of key signalling proteins within these areas based on fluorescence microscopy data at single-molecule resolution

Table S2 | Quantitative characterization of close contacts between T cells and rCD2-SLB and the organization of key signaling proteins within these areas based on fluorescence microscopy data at single-molecule resolution

Table S3 | Parameters used for Model 1 to derive the analysis shown in Figure 3 and 4

Table S4 | Parameters used for Model 2 to derive the analysis shown in Figure S6 and S7

III. Supplementary Figures

Figure S1 | Analysis of the distribution of molecules at close-contacts between T cells and glass surfaces by TIRF microscopy and single-particle tracking.

Figure S2 | Quantitative analysis of CD45 and Lck density and TCR diffusion at close-contacts between T cells and glass surfaces by single-particle tracking.

Figure S3 | CD45 segregates from close-contacts between T cells and glass surfaces at sub-μm length scales in a process that is independent of ATP and other cell-specific components.

Figure S4 | Simultaneous detection of close contact formation and calcium release on Jurkat T cells interacting with IgG-coated glass surfaces.

Figure S5 | Dependence of the mathematical description of the KS model for TCR triggering on various parameters and testing the validity of assumptions made (Model 1).

Figure S6 | Ligand-independent TCR triggering depends on close contact area and duration (Model 2).

.

bioRxiv preprint doi: https://doi.org/10.1101/109785; this version posted February 19, 2017. The copyright holder for this preprint (which was not certified by peer review) is the author/funder. All rights reserved. No reuse allowed without permission.

Figure S7 | TCR signalling depends on ligand-binding and LIT may play a role in signalling amplification (Model 2).

Figure S8 | Number and fraction of triggered TCRs for a single close contact radius in both the presence and absence of agonist pMHC.

Figure S9 | The presence of SLB-bound CD45-RABC ectodomain inhibits contact formation of CD48+ Jurkat T-cells with rCD2 SLBs.

IV. Supplementary Movies

Movie S1 | Single-molecule tracking data (CD45, TCR; IgG-coated glass)

Movie S2 | Close contact growth

Movie S3 | Single-molecule tracking data (CD45; rCD2-SLB)

Movie S4 | Ca^{2+} release as measured by change in Fluo-4 fluorescence in Jurkat T-cells forming contacts depleted of CD45 with glass (close-contacts visualized by interference reflection microscopy)

Movie S5 | Ca^{2+} release as measured by change in Fluo-4 fluorescence in Jurkat T-cells forming contacts depleted of CD45 with CD2 (labeled) -containing SLBs

Movie S6 | Ca^{2+} release as measured by change in Fluo-4 fluorescence in J.RT3-T3.5 T-cells forming contacts depleted of CD45 (labeled) with CD2-containing SLBs

Movie S7 | Animation of the changes in the TCR probability density across a growing close contact over time corresponding to the modelling shown in Figure 3E

Movie S8 | Loss of contact formation between Jurkat T-cells and CD2-containing SLBs by the addition of CD45 to the SLBs

Movie S9 | CD45-RABC spontaneously segregates from CD2-mediated close-contacts formed by Jurkat T-cells (CD48+) with CD2- and CD45RABC-containing SLBs

bioRxiv preprint doi: https://doi.org/10.1101/109785; this version posted February 19, 2017. The copyright holder for this preprint (which was not certified by peer review) is the author/funder. All rights reserved. No reuse allowed without permission.

STAR Methods

Contact for reagents and resource sharing

As lead contact, David Klenerman is responsible for all reagents and resource requests. Please contact David Klenerman at dk10012@cam.ac.uk with requests and enquiries.

Experimental model and Subject details

Cell lines

Human Jurkat T cells (clone E6-1) and J.RT3-T3.5 were obtained from ATCC (ATCC®TIB-152™). All other cell lines were transduced with lentivirus to express gene of choice. Human HEK293T were obtained from ATCC (ATCC® CRL-3216™). T Cells were cultured in sterile RPMI (Sigma Aldrich) supplemented with 10% FCS (PAA), 2 mM L-Glutamine (Sigma Aldrich), 1 mM Sodium Pyruvate (Sigma Aldrich), 10mM HEPES (Sigma Aldrich), and 1% Penicillin-Streptomycin-Neomycin solution (Sigma Aldrich). HEK293T cells were cultured in sterile DMEM (Sigma Aldrich) supplemented with 10% FCS (PAA), 2mM L-Glutamine (Sigma Aldrich) and 1% Penicillin-Streptomycin (Sigma Aldrich) at 37˚C and 5% CO_2 and were maintained between 10% to 90% confluency. Cells were maintained at 37˚C and 5% CO_2 during culturing, and handling was performed in HEPA-filtered microbiological safety cabinets. Typically, cells were kept at a density between 5-9 x 10^5 cells/ml. The UCHT1 hybridoma was a generous gift from Dr Neil Barcley, Sir William Dunn School of Pathology, University of Oxford and the GAP8.3 hybridoma was obtained from ATCC (HB-12™). Hybridoma cells were cultured in sterile DMEM (Sigma Aldrich) supplemented with 10% FCS (PAA), 2mM L-Glutamine (Sigma Aldrich) and 1 mM Sodium Pyruvate (Sigma Aldrich) at 37˚C and 5% CO_2 and were maintained between 10% to 90% confluency. All cells used throughout this study were regularly tested for mycoplasma.

Method details

Plasmids

For HA-CD45-Halo, LCK-Halo, and TCRβ-Halo (New England Biolabs, UK) the genes were amplified by PCR to produce dsDNA fragments encoding proteins of interest flanked at the 3′ end by a sequence coding for a Gly-Ser linker which was followed by Halo-tag. Following confirmation of sequence and reading frame integrity the Lck-Halo and TCRβ-Halo were sub-cloned into the lentiviral pHR-SIN plasmid. To generate mm-Lck the appropriate residues were mutated by a PCR amplification reaction using forward and reverse oligos encoding the desired mutation. Sequence integrity was confirmed by reversible terminator base sequencing.

Generation of stable transduced cell lines

Jurkat derived T cell lines stably expressing either mCitrine-actin, LCK-Halo, and TCRβ-Halo were generated using a lentiviral transduction strategy. HEK293T cells were plated in 6-well plates at 6 x 10^5 cells per well in DMEM (Sigma Aldrich), 10% FCS (PAA) and antibiotics. Cells were incubated at 37 ˚C and 5% CO_2 for 24h before transfection with 0.5 µg/well/plasmid of the lentiviral packaging vectors p8.91 and pMD.G (2nd generation) and the relevant pHR-SIN lentiviral expression vector using

bioRxiv preprint doi: https://doi.org/10.1101/109785; this version posted February 19, 2017. The copyright holder for this preprint (which was not certified by peer review) is the author/funder. All rights reserved. No reuse allowed without permission.

GeneJuice® (Merck Millipore) as per the manufacturer's instructions. 48 h post transfection, the supernatant was harvested and filtered using a 0.45 µm Millex®-GP syringe filter unit to remove detached HEK293T cells. 3ml of the lentiviral-conditioned medium was added to 1.5 x 10^6 Jurkat T cells.

Sample preparation for Calcium response measurements

25mm diameter coverslips (SLS) were coated with 500ul of 50 µg/ml donkey anti-mouse IgG antibody, or bovine IgG (Sigma Aldrich), in coating buffer (50 mM Na_2CO_3, 50 mM $NaHCO_3$, pH 9.6, filtered using a 0.22 µm Millex®-GP syringe filter unit) for at least 30 min. Coverslips were washed a final time with 3 x 1 ml HBS before use. Jurkat T-cells were labeled with 4 µM Fluo-4 AM (F-14201; Invitrogen, Paisley UK) for 30 min at room temperature with 2.5 mM probenecid (P-36400; Invitrogen, Paisley UK) in RPMI (Sigma-Aldrich, UK) without supplements. Cells were then washed in HBS (51558; Sigma, UK) and the medium changed to HBS containing 2.5 mM probenecid before their addition to the microscope sample container with the prepared microscope coverslip.

Calcium response measurements only (Figure 3a-c and 4e)

Jurkat T cells were labeled with 4 µM Fluo-4 AM (F-14201; Invitrogen, Paisley UK) for 30 min at room temperature with 2.5 mM probenecid (P-36400; Invitrogen, Paisley UK) in RPMI (Sigma-Aldrich, UK) without supplements. Cells were then washed in HBS (51558; Sigma, UK) and the medium changed to HBS containing 2.5 mM probenecid before their addition to the microscope sample container with the prepared microscope coverslip. Cells were imaged at 37°C and 5% CO_2 using a 10x air objective on the spinning disk confocal microscope (Zeiss Cell Observer Spinning Disc Confocal), 488 nm laser excitation and fluorescence detection around 530 nm, with an exposure time of 350 ms and a time between frames of 500 ms for 840 frames.

We used a modified version, CalQuo2.0, of CalQuo (Fritsche et al. 2015), to detect single-cells landing events on the prepared coverslip surfaces, and to record fluorescence intensities over time at the coverslip surface. Briefly, for each cell, stable changes in fluorescence intensity above background levels were indicative of the cell 'landing' and calcium responses associated with Jurkat T-cell signalling (>2.5 fold fluorescence intensity above 'landing' intensity). For each cell, the time lapse between 'landing' and 'signaling' was also determined. All cells were individually analysed and the fraction of signalling cells was determined from the total number of cells detected after landing, provided that cells landed before frame 480, in order to allow 3 minutes for signalling to occur. CalQuo2.0 Matlab script is available upon request from ricardfe@stanford.edu (R.A.F) and dk10012@cam.ac.uk (D.K.).

Calcium response measurements combined with interference reflection microscopy (IRM) and subsequent image analysis

IRM experiments were performed at 37°C and 5% CO_2 with a 1.4 NA 63x oil-immersion objective on a scanning laser confocal microscope (Zeiss780, Carl Zeiss AG). To detect IRM we used a 647 nm laser, a NT80/20 neutral beam splitter (20% excitation reflected, 80% emission transmitted), and a GaAsP

bioRxiv preprint doi: https://doi.org/10.1101/109785; this version posted February 19, 2017. The copyright holder for this preprint (which was not certified by peer review) is the author/funder. All rights reserved. No reuse allowed without permission.

detector operated in reflection mode. IRM images were recorded at a frame repetition of 6.52 s and simultaneously combined with fluorescence imaging of calcium responses using Fluo-4 (excited at 488 nm and detection at ~530 nm) together with differential-interference-contrast (DIC) imaging using the microscope's TPMT module for observation of the cell body in a ZEISS LSM 710 microscope setup. The IRM and Fluo-4 image sequences were analyzed using custom-written MATLAB code. Briefly, cell position was detected in the last frame by applying an intensity threshold in the Fluo-4 channel, and for each cell its mean intensity trace across the entire image sequence was calculated. The time of landing (t_{land}) and Ca^{2+} release (t_{Ca}) were determined in a semi-automated fashion from these intensity traces, and the time taken to trigger defined as t_{Ca} - t_{land}. For the interval t_{land} to t_{Ca}, the area of cell-surface contact was calculated for each cell for all frames of the IRM image sequence. The intensity threshold required to discriminate cell contacts over the (lighter) background was defined empirically; we defined cell-surface contacts as areas of intensities below the mean of the 100 brightest pixels of the image. From this analysis, we obtained the change of cell-surface contact area for individual cells until the time point of Ca^{2+} release t_{Ca}. All further statistical analysis and fits of the traces were performed with Origin (OriginPro 9.1 G, OriginLab Corporation, Northampton, USA).

Fab preparation and labeling

The TCR on Jurkat T cells was labeled with Alexa Fluor 647 Fab (UCHT1, anti-CD3ε; purified from hybridoma supernatant). The CD45 was labeled with Alexa Fluor 488 Fab (Gap8.3, anti-CD45; purified from hybridoma supernatant). Both Fabs were prepared from purified antibody using immobilized papain (agarose resin, ThermoFisher and per manufacturer protocol). Fab digestion and purity was confirmed by size exclusion chromatography. For Fab labeling, Alexa Fluor 488 and Alexa Fluor 647 antibody labeling kit (ThermoFisher) was used as per manufacturer protocol. For cell labeling, 1 ml of 5 x 10^5 cells/ml were incubated with Fab (1-10 nM) on ice for 25 minutes. Cells were washed three times in 20 nm filtered PBS.

Fluorescence-activated cell sorting and quantification of protein expression

Wild type or transduced Jurkat and HEK293T cells were washed once in ice-cold PBS, and 1 million cells were incubated with appropriate antibodies (isotype control, eBioscience, UK; Gap 8.3, purified from hybridoma cells; anti-HA, clone HA-7, Sigma Aldrich; UCHT1, purified from hybridoma) at 10 ug/ml for 30 min on ice in PBS/0.05% Azide, washed once in PBS and incubated with a fluorescently labeled secondary anti-mouse antibody as appropriate (alexa 647 or alexa 488, Molecular Probes, Invitrogen or PE-conjugated, Sigma Aldrich) for a further 30 min on ice. Cells were washed in ice-cold PBS and analysed on a Beckman Coulter CyAn Analysers. For quantification of cell surface protein expression QuantiBrite-PE beads (BD Biosciences) were used as per manufacturer instructions. Mean fluoresce intensity analysis and further data processing was performed with FlowJo software using a standard gate on live cells based on the forward- and side-scatter profile.

bioRxiv preprint doi: https://doi.org/10.1101/109785; this version posted February 19, 2017. The copyright holder for this preprint (which was not certified by peer review) is the author/funder. All rights reserved. No reuse allowed without permission.

HaloTag® labeling

Cells expressing HaloTag® (Promega, UK) fusion protein were labeled with TMR Cell * following manufacturer's preparation protocol (www.promega.co.uk/products/imaging-and-immunological-detection/cellular-imagingwithhalotag/proteintrafficking). First, the cell medium was replaced with 200 µl RPMI without supplements to which 1-5 µM of Halo-Tag TMR dye was added and cells were incubated at 37°C for 45 minutes. To ensure that free dye would not remain in the cytoplasm, cells were washed three times in HBS and then further incubated 37°C for 30 minutes followed by another three washes with PBS.

Total internal reflection microscopy (TIRFM)

For Figure 1I: A collimated 640 nm (LaserBoxx 641, Oxxius, Lannion, France) laser beam was focused at the back aperture of a 60x oil TIRF objective (Olympus, NA 1.49, UIS2 series APON 60XOTIRF) mounted on an IX71 Olympus inverted microscope frame. The power of the collimated beams at the back aperture of the microscope was 20 mW. Emitted fluorescence was collected by the same objective, separated from the excitation by a dichroic (Di01-R4-5/488/561/635, Semrock), expanded through a 2.5x achromatic beam expander (Olympus, PE 2.5x 125) and sent through an emission filters 635 long-pass filter (Semrock, BLP01-635R). The images were recorded on an EM-CCD camera (Evolve 512, Photometrics) operating in frame transfer mode at -80°C. Videos of 1000 frames were acquired at exposure times of 30 ms using Micromanager.

For all other Figures containing TIRF data: TIRF imaging was performed using total internal reflection fluorescence microscopy (TIRFM). A diode laser operating at 488 nm (20mW, Spectra Physics, Newport, US) and either a diode laser operating at 561 nm (Excelsior, 20mW, Spectra Physics, Newport, US) or a HeNe laser operating at 633 nm (25LHP991230, Melles Griot) were directed into a TIRF objective (60x Plan Apo TIRF, NA 1.45, Nikon Corporation, Tokyo, Japan) mounted on an Eclipse TE2000-U microscope (Nikon Corporation, Tokyo, Japan) parallel to the optical axis and offset in order to achieve total internal reflection of the beam. The emitted fluorescence was collected by the same objective and separated from the returning TIR beam by a dichroic mirror (FF500/646-Di1, 488/633 emission, Semrock, US) or (XF2044-490-575DBDR, 488/561 emission, Omega Optics). The green fluorescence emission was subsequently separated from the red fluorescence emission by a second dichroic mirror and filter sets; for excitation with 488 and 633: FF605-Di02 (Dual-View mounted, Photometrics, Roper Scientifics, US), FF03-525/50-25 (488 emission), BLP01-635R-25 (633 emission), all Semrock, US; for excitation with 488 and 561: FF562-Di03 (Dual-View mounted, Photometrics, Roper Scientifics), FF02-525/40-25 (488 emission), LP02-568RS-25 (561 emission), all Semrock, US. The fluorescence signals from both channels were simultaneously recorded using an EM-CCD camera (Cascade II: 512, Photometrics, Roper Scientifics, US) operating at -70 °C, whereby each color was recorded on one half of the EMCCD chip. A grid consisting of regularly spaced ion-beam etched holes in gold-on-glass was used to achieve image registration across both emission channels. The Dual-View

bioRxiv preprint doi: https://doi.org/10.1101/109785; this version posted February 19, 2017. The copyright holder for this preprint (which was not certified by peer review) is the author/funder. All rights reserved. No reuse allowed without permission.

optics were adjusted to maximize the overlap of the grid images in the two channels under bright field illumination, resulting in a mean alignment precision of approximately 120 nm. Data were acquired using either single snap shots or time-lapse acquisition using Micromanager (Edelstein et al., 2010).

Supported Lipid Bilayers (SLB) preparation

Prior to SLB formation on glass cover slips, the cover slips (size no. 1: 0.13 mm in thickness, VWR International, UK) were cleaned by incubation in Piranha solution (3:1 sulfuric acid: hydrogen peroxide) for 1 hour followed by thorough rinsing with ultrapure water (MilliQ, 18.2 MΩ resistance) and subsequent plasma cleaning for 15 minutes (Argon, PDC-002, Harrick Plasma). Lipid vesicles were prepared by extrusion through a 50-nm membrane (Whatman, Maidstone, UK) using an Avanti Mini-Extruder (Avanti Polar Lipids, Alabaster, AL). The vesicles consisted of 1-palmitoyl-2-oleoyl-sn-glycero-3-phosphocholine (POPC) with either 0 or 5.0 wt% of 1,2-di-(9Z-octadecenoyl)-sn-glycero-3-[(N-(5-amino-1-carboxypentyl)imino-diaceticacid)succinyl] (nickel salt) (18:1 DGS-NTA(Ni), both Avanti Polar Lipids, Alabaster, USA). POPC vesicles containing 0.01 wt% Oregon Green 488 1,2-dihexadeca-noylsn-glycero-3-phosphoethanolamine (OG-DHPE) were also used for some of the experiments in this work. The buffer solution used in the experiments was HBS buffer (10mM 2-[4-(2-hydroxyethyl)piperazin-1-yl]ethanesulfonic acid (HEPES), 150mM NaCl), adjusted to a pH of 7.4, filtered through a 0.2 µm membrane (AnaChem, Luton, UK) before use. Press-to-seal silicone isolators (4.5mm diameter, Grace Bio-Labs, Bend, Oregon, USA) were pressed on the cleaned cover slips, following the manufacturer's instructions, to form SLBs within the silicon wells of the isolator by adsorption and subsequent rupture of the lipid vesicles prepared by placing a 20 µl drop of the vesicle solution (1 mg/mL lipids) on the glass surface. After the formation of an SLB from the lipid vesicle suspension (~30min) the vesicle solution was first replaced with buffer solution and then with a solution containing 0.25µg/mL of rCD2-6His-spacer-6His. For some experiments, the rCD2 molecules were labeled with Alexa Fluor 488 or 647 (Molecular Probes, Invitrogen, UK) via surfaced exposed lysines. Ni_2^+-NTA lipids were incubated with rCD2 in the SLB for 60 minutes after which the binding of proteins had reached equilibrium.

Sample preparation for imaging (TIRFM experiments)

Before imaging, approximately 10^6 cells were resuspended in PBS (phosphate buffered saline, pH 7.4) and incubated in a microcentrifuge tube with the desired antibody fragments (as indicated in the text) for 30 min at room temperature (22°C). After the incubation step, the cells were washed three times with PBS by centrifugation and resuspension of the pellet (600×g, 2 min) and transferred to glass cover slips (cleaned by exposure to Argon plasma for 30 min (PDC-002; Harrick Plasma, US), and subsequently coated with a solution of bovine IgG (Sigma-Aldrich) at a concentration of 10 µg/mL or an SLB for imaging. After the slides were transferred to the microscope stage, cells were added and imaging was carried out within the first minutes following cell attachment room temperature.

bioRxiv preprint doi: https://doi.org/10.1101/109785; this version posted February 19, 2017. The copyright holder for this preprint (which was not certified by peer review) is the author/funder. All rights reserved. No reuse allowed without permission.

Image analysis (TIRFM experiments)

Image analysis was performed using a combination of manual analysis (ImageJ, U. S. National Institutes of Health, Bethesda, Maryland, USA, http://imagej.nih.gov/ij/)) and custom-written MATLAB code (MATLAB R 2014b, The MathWorks, Natick, US).

i. Image acquisition and analysis (single-molecule tracking experiments for close-contacts on glass, Figure 1)

Videos were obtained at a frames rate of 28.6 frames per second (exposure time: 33ms) simultaneously visualizing the distribution of wtCD45 (labeled with high FAB concentrations as described above) in one channel and trajectories of either wtCD45, HA-CD45-Halo, (mm)Lck-Halo or TCR-β-Halo in the second channel. The videos were manually cropped to the region of a single cell, and average images of the CD45 distribution obtained by an average Z-projection in ImageJ over 200 frames. The contours of the close-contacts were manually traced in the averaged images by following the line of maximum CD45 fluorescence around a contact with an n-sided polygon using the Region-of-Interest (ROI) manager in ImageJ. The videos for the second channel (recording the trajectories of single molecule in the close-contacts) were analysed using the custom-written software (MATLAB) described in Weimann et al. The positions of the trajectories obtained were then mapped onto binary representations of the contacts (created by converting the ROI regions obtained from manually-tracing the contacts' boundaries in ImageJ into binary masks) using a custom-written MATLAB routine. Using these binary images, the routine also sorted the trajectories into two categories ("confined within" and "outside" the contact). The diffusion coefficients for those two categories were trajectories were extracted as described elsewhere (Weimann et al. 2013).

ii. Image acquisition and analysis (single-molecule tracking experiments for close-contacts on SLBs, Figure 1)

Videos were obtained at a frames rate of 28.6 frames per second (exposure time: 33ms) simultaneously visualizing the distribution of wtCD45 (labeled with high FAB concentrations as described above) in one channel and trajectories of either wtCD45, HA-CD45-Halo, (mm)Lck-Halo or TCR-β-Halo in the second channel. Videos were analyzed using custom-written software (MATLAB). An interactive user interface allowed the user to select boundaries for each cell based on bright field images acquired during the data collection phase. Binary masks of the CD45 distribution for the selected cells were obtained by an average Z-projection over 200 frames in the CD45 channel, and applying an intensity threshold to the image (pixels were assigned a value of 1 if their intensity values I fulfilled the condition $I > (\mathrm{mean}(I_{region}) - 2 * \mathrm{std}(I_{region}))$. The videos for the second channel (recording the trajectories of single molecule in the close-contacts) were analyzed as described in *i*. Trajectory numbers "confined within" and "outside" the contact and diffusion coefficients were

bioRxiv preprint doi: https://doi.org/10.1101/109785; this version posted February 19, 2017. The copyright holder for this preprint (which was not certified by peer review) is the author/funder. All rights reserved. No reuse allowed without permission.

extracted as described in *i.* The number of classified trajectories for a given cell was normalized by the corresponding mask area, i.e. the area "inside" and "outside" the contact, respectively.

iii. Image acquisition and analysis (simultaneous imaging of CD45 distribution in the close-contacts on SLBs and Ca^{2+} signaling / Fluo-4 fluorescence increase with TIRFM, Figure 2 and 4)

Data (videos) were acquired on the TIRF microscope described in section Total internal reflection microscopy at 37°C, using the 488 and 633 lasers for excitation and the corresponding dicroics and emission filters. Data were acquired using alternating excitation and time-lapse acquisition, with an exposure time of 100 ms, and a time between frames of 2 s. The videos were analyzed using custom-written MATLAB code. Briefly, cell positions were manually traced in the last frame of the Fluo-4 channel, and for each cell its mean intensity trace across the entire image sequence was calculated. The time of landing (t_{land}) and Ca^{2+} release (t_{Ca}) were determined in a semi-automated fashion from these intensity traces, and the time taken to trigger defined as t_{Ca} - t_{land}. For the interval t_{land} to t_{Ca}, the area of cell-surface contact was calculated from the CD45 channel for each cell by manually tracing the area inside the close contact outlined by CD45 fluorescence in a program-integrated GUI. From this analysis, we obtained the change of cell-surface contact area for individual cells until the time point of Ca^{2+} release t_{Ca}. All further statistical analysis and fits of the traces were performed with Origin (OriginPro 9.1 G, OriginLab Corporation, Northampton, USA).

iv. Image acquisition and analysis (close-contacts formation of cells on SLBs containing rCD2 and RABC-CD45 and Ca^{2+} signaling / Fluo-4 fluorescence increase with TIRFM, Figure 3)

Data (videos) were acquired on the TIRF microscope described in section Total internal reflection microscopy at 37°C, using the 488 and 633 lasers for excitation and the corresponding dicroics and emission filters. Data were acquired using alternating excitation with an exposure time of 100 ms, and, if time lapse acquisition was used, a frames rate of 0.5 frames s^{-1}. Snap shots were taken of cells ~10 minutes after landing on the SLB. To determine the fraction of contact-forming cells, images were analyzed using custom-written MATLAB code. Briefly, cell positions were manually traced in the Fluo-4 channel, and for each cell its mean intensity over the background was calculated. Cells were counted to have formed a stable contact with the rCD2 in the SLB if the contact intensity was greater than 2-times the intensity of the background. The time-lapse videos were analyzed to obtain the fraction of cells that released Ca^{2+} and the time taken by cell to trigger as described in *iii*.

v. Super-resolution microscopy of CD45 distribution in Jurkat T cells (Figure 1I)

1. CD45 was a labeled with Gap8.3 conjugated to the fluorescent dye Atto655 and made to emit intermittently by the addition of ascorbic acid (100μM; for details see Vogelsang et al., 2009)

). Movies of isolated fluorescent puncta could thus be obtained whose center positions were extracted using the software PeakFit (www.sussex.ac.uk/gdsc/intranet/microscopy/imagej/smlm_plugins), an

bioRxiv preprint doi: https://doi.org/10.1101/109785; this version posted February 19, 2017. The copyright holder for this preprint (which was not certified by peer review) is the author/funder. All rights reserved. No reuse allowed without permission.

ImageJ plug-in for super-resolution analysis. Briefly, local maxima in each frame were fitted with a 2D-Gaussian described by seven parameters (position on two axes, standard deviation on two perpendicular axes and angle to the horizontal axis, amplitude, and offset). Finally, each single-molecule position was re-plotted using a custom macro written in ImageJ (http://rsb.info.nih.gov/ij/) as a 2D Gaussian profile defined by the measured integrated intensity and a width given by the average statistical error in localization of the centre (95% confidence interval, averaged over all single-molecule localizations; for further details see (Ptacin et al., 2010)

Modelling

All plots for the theoretical modelling of TCR triggering were generated in MATLAB (MATLAB R 2014b, The MathWorks, Natick, US) using the equations derived in the Quantitative modeling of TCR triggering section.

Quantitative modeling of TCR triggering

Both Model 1 and Model 2 seek to mathematically describe TCR behavior in close contact zones (CCZs); corresponding to close contacts described in Chang *et al.* and this study). Our experiments find that these contacts are initially small and grow over time (see also Figure S1 and Movie S2). Cell-cell contacts are known to be very transient in the absence of signaling. Since we are interested in signal initiation, we assume that CCZs form for finite periods (referred to as the contact duration).

In contrast to other models, the kinetic segregation (KS) model proposes that receptor triggering requires only that the TCR stays accessible to kinases within CCZs, protected from phosphatases that would otherwise terminate signaling, and for TCR phosphorylation to be sufficiently long-lived for downstream effects to be initiated. pMHC ligands, *via* trapping effects, serve only to increase the residence time of the TCR inside the CCZ (Davis and van der Merwe, 1998; Davis et al. 2006). We therefore assume for our modeling (1) that when a CCZ is formed, TCRs can diffuse in and out of the contact, and (2) that if the TCR binds to ligand within the CCZ, it continues to diffuse within the CCZ but is unable to leave. Any TCR that remains in the CCZ for longer than 2 seconds, irrespective of its binding status, is assumed to be triggered (see also discussion in the results section). The models can be used to calculate how TCR triggering probability is affected by CCZ size, growth and duration, and by ligands presented at different densities and affinities.

Model 1 calculates TCR density across the CCZ based on the rate of TCR entry into the CCZ (for a given CCZ radius, initial TCR density and TCR diffusion coefficient). Therefore, it can also accounts for changes in TCR entrance rate and in the dwell-time of TCRs already present inside the CCZ as the CCZ grows. This approach potentially yields more accurate calculations, but requires moving-boundary coupled partial differential equations that are computationally expensive.

bioRxiv preprint doi: https://doi.org/10.1101/109785; this version posted February 19, 2017. The copyright holder for this preprint (which was not certified by peer review) is the author/funder. All rights reserved. No reuse allowed without permission.

Model 2 assumes a uniform distribution of TCRs inside the close contact at all times and, as the contact grows the numbers of TCRs inside the contacts is updated using the initial, assumed TCR density in the CCZ. This approach is more intuitive and simplifies the calculations since they only require the use of ordinary differential equations. For small contacts, and in the case of slow CCZ growth rates compared to TCR diffusion, as observed experimentally, the assumptions are applicable.

Model 1: Modelling of receptor triggering using moving-boundary coupled partial differential equations to account for close contact growth

See Figures 3 and 4 and Figure S5

a. Model formulation

Since CCZs grow on time-scales similar to the diffusion of the TCR, changes in TCR density in CCZs need to be described by a coupled system of moving-boundary partial differential equations (PDEs),

$$\begin{aligned} \partial T/\partial t &= D_T \nabla^2 T - k_{\text{on}}^* T + k_{\text{off}} C, 0 < |\mathbf{r}| < R(t; t_{\text{entry}}); \\ \partial C/\partial t &= D_C \nabla^2 C + k_{\text{on}}^* T - k_{\text{off}} C, 0 < |\mathbf{r}| < R(t; t_{\text{entry}}), \end{aligned} \qquad \text{(equation 1.1)}$$

where $T(\mathbf{r}, t; t_{\text{entry}})$ and $C(\mathbf{r}, t; t_{\text{entry}})$ represent free and ligand-complexed TCRs diffusing with coefficient $\mathrm{D_T}$ and $\mathrm{D_C}$, respectively, and with the receptors undergoing reversible binding with first-order rates (k_{on}^*,$\mathrm{k_{off}}$). Note that $k_{on}^* = \mathrm{k_{on}}[\mathrm{M}]$ where $\mathrm{k_{on}}$ is the bimolecular on-rate (in units of $\mu m^2/s$) and $[\mathrm{M}]$ is the ligand concentration (in units of μm^{-2}). The boundary conditions for the disc domain of radius R are adsorbing for T and no flux for C,

$$\begin{aligned} T(R) &= 0, \\ D_C \nabla C \cdot \hat{\mathbf{n}} + R'(t) C &= 0 \end{aligned} \qquad \text{(equation 1.2)}$$

Importantly, the domain area grows linearly in time and therefore,

$$R(t; t_{\text{entry}}) = \sqrt{R_0^2 + g(t + t_{\text{entry}})/\pi} \qquad \text{(equation 1.3)}$$

where g is the growth rate (in units of $\mu m^2/s$) and t is time. The initial conditions at $t = t_{entry}$ are as follows,

$$\begin{aligned} T(r) &= \delta(\mathbf{r} - \mathbf{r_0}); \\ C(r) &= 0, \end{aligned} \qquad \text{(equation 1.4)}$$

bioRxiv preprint doi: https://doi.org/10.1101/109785; this version posted February 19, 2017. The copyright holder for this preprint (which was not certified by peer review) is the author/funder. All rights reserved. No reuse allowed without permission.

where $r_0 = (R_0 - \varepsilon, \theta)$. The additional term $R'(t)C$, which reflects the rate of growth in the region, is a necessary addition to the usual Neumann condition in order to prevent mass of C leaving the domain. To see this, consider the change in total mass $M(t) = \int_{\Omega(t)} (T + C)\, dr$,

$$M'(t) = \frac{d}{dt}\int_0^{2\pi}\int_0^{R(t)} (T + C)\, r dr d\theta \quad = RR'\int_0^{2\pi} [T + C]_{r=R}\, d\theta + \int_0^{2\pi}\int_0^{R(t)} \frac{d}{dt}(T + C)\, r dr d\theta,$$

$$= \int_0^{2\pi} [RR'(T + C) + R(D_T T_r + D_C C_r)]_{r=R}\, d\theta$$

$$= R\int_0^{2\pi} [D_C C_r + R'C]_{r=R}\, d\theta + D_T R\int_0^{2\pi} [T_r]_{r=R}\, d\theta$$

(equation 1.5)

The flux of T-cell receptors in complex (C) through the boundary should be zero which gives rise to the boundary condition. In the case of modeling CCZs of fixed size (Fig. 3B-E), $g = 0$ in equation 1.3.

b. Model output

The output of the model is the probability (P_s) that a single receptor has remained within the CCZ for more than 2 seconds, for contact duration (t_f),

$$P_s(t_{\text{entry}}) = \int_{\Omega(2;t_{\text{entry}})} T(\mathbf{r}, 2; t_{\text{entry}}) + C(\mathbf{r}, 2; t_{\text{entry}})\, d\mathbf{r}. \qquad \text{(equation 1.6)}$$

The time-dependent rate of TCR entry into the domain ($k_t(t)$) is expected to be proportional to the size of the domain, which increases over time. Using previously derived results (see Equations 11 in Weaver, 1983), we find,

$$k_t(t) = \frac{4\pi D T_m}{\log\left(A/(\pi R(t)^2) - 1\right)} \qquad \text{(equation 1.7)}$$

where $A = 415\,\mu m^2$ is the cell surface area, $T_m = 100\,\mu m^{-2}$ (varied over the simulations; see also Table S3) is the TCR density far away from the CCZ, and $D_T = 0.05\,\mu m^2/s$ (varied over the simulations, see also Table S3) is the TCR diffusion coefficient. With these numbers, we find that the rate of TCR entry into the domain (k_t) increases from $\approx 4\,s^{-1}$ to $\approx 18\,s^{-1}$ as the domain radius increases from 0.01 μm to 2 μm.

Given that multiple receptors can enter the CCZ during the contact duration (t_f), we need to calculate the probability that at least one TCR has remained within the domain for more than 2 s (P_m, referred to as "triggering probability"). The number of TCRs that have entered the domain in time interval $[t_i, t_i + \Delta t]$ can be estimated as $k_t(t_i)\Delta t$ so that P_m is estimated as follows,

bioRxiv preprint doi: https://doi.org/10.1101/109785; this version posted February 19, 2017. The copyright holder for this preprint (which was not certified by peer review) is the author/funder. All rights reserved. No reuse allowed without permission.

$$P_m = 1 - \prod_{i=1}^{N} [1 - P_s(t_i)]^{k_t(t_i)\Delta t} . \qquad \text{(equation 1.8)}$$

In the case where P_s and k_t are constants:

$$P_m = 1 - \prod_{i=1}^{N} [1 - P_s]^{k_t \Delta t} = 1 - [1 - P_s]^{k_t N \Delta t} = 1 - [1 - P_s]^{k_t (t_f - 2)} \qquad \text{(equation 1.9)}$$

For the calculation of the number of TCRs expected to stay for >2 s within the CCZ in the absence of growth ($g = 0$, Figure 3C), a term is included in the expectation representing the initial number of TCRs in the CCZ at $t = 0$,

$$T_m \pi R^2 \times P_s(t = 0) + \sum_i k_t(t_i) \Delta t \times P_s(t_i) \qquad \text{(equation 1.10)}$$

bioRxiv preprint doi: https://doi.org/10.1101/109785; this version posted February 19, 2017. The copyright holder for this preprint (which was not certified by peer review) is the author/funder. All rights reserved. No reuse allowed without permission.

Model 2: Modelling of receptor triggering assuming a uniform distribution of TCRs inside close contacts, using ordinary differential equations

See Figures S6 and S7

This model does not incorporate the effect of CCZ growth on the TCR entrance rate ($k_t(t)$) into the CCZ, and assumes that the TCR is randomly and uniformly distributed with density T_m across the entire contact. The mean time an unbound TCR resides in the CCZ is given by $r^2/(8D)$, where *r* is the radius of the CCZ and *D* is the diffusion coefficient (Wofsy et al. 2001). The mean time taken for a TCR to find a pMHC is: $1/(k_{on}M)$ where k_{on} is the 2D on-rate and M is the density of pMHCs (Jansson 2010). Dividing $r^2/(8D)$ with $1/(k_{on}M)$ gives the number of TCR/pMHC engagements before the TCR diffuses out of the CCZ. Multiplying the number of engagements with the lifetime of the TCR-pMHC complex ($1/k_{off}$) allows calculation of the mean residence time of TCRs in the CCZ

$$\tau = \frac{r^2}{8D}(1 + KM)\ , \qquad \text{(Equation 2.1)}$$

where K is the association constant (k_{on}/k_{off}) for pMHC. Assuming a uniform distribution of TCRs across the contact, for a freely-diffusing TCR the residence time in the CCZ of unbound TCRs assumes an exponential distribution and the probability that an unbound TCR ($K = 0$ in equation 2.1) stays within the CCZ for longer than t_{min} seconds is

$$P_s = e^{-t_{min}/\tau} = e^{-t_{min}/\frac{r^2}{8D}} = e^{-t_{min}/\frac{A}{\pi 8D}} \qquad \text{(Equation 2.2)}$$

(Equation 2.2)

where A is the area of a circular CCZ ($A = \pi r^2$).

Equation 2.2 predicts the probability that a TCR stays longer than t_{min} seconds for a CCZ of fixed size. To account for increases in size with time, the area (A) can be substituted by the product of growth rate (g) and time ($A = g \cdot t$; assuming a uniform distribution of the TCR):

$$P_s = e^{-t_{min}/\frac{g \cdot t}{\pi 8D}} \qquad \text{(Equation 2.3)}$$

To derive the relationship between time to triggering (t_{trigg}) and growth rate (g), equation 2.3 can be reformulated as:

$$t_{trigg} = -\frac{t_{min}}{\log(P_s)}\frac{\pi 8D}{g} \qquad \text{(Equation 2.4)}$$

While the probability (P_s) that a single unbound TCR stays longer than 2 seconds (t_{min}) in the CCZ can be calculated using equation 2.2, the probability that a given number k of unbound TCRs are triggered (*i.e.* stay longer than 2 seconds in the CCZ) can be calculated from the binomial distribution:

$$P_k = \binom{n}{k} {P_s}^k (1 - P_s)^{n-k}, \qquad \text{(Equation 2.5)}$$

bioRxiv preprint doi: https://doi.org/10.1101/109785; this version posted February 19, 2017. The copyright holder for this preprint (which was not certified by peer review) is the author/funder. All rights reserved. No reuse allowed without permission.

where k is number of successes (*i.e.* triggered TCRs), n is the number of TCRs that have entered within the CCZ t_f; $n = \left(\frac{t_f}{\tau}\right) \cdot T_m * A)$ and P_S is the probability of a success (given by equation 2.2). Therefore, the probability that at least one TCR (k = 1 or greater) stays longer than 2 seconds in the CCZ (*i.e.* the "Triggering probability", see also **Model 1**) is

$$P_m = 1 - \binom{n}{k} P_s{}^k (1 - P_s)^{n-k} \qquad \text{(Equation 2.6)}$$

where *k* is 0 (the number of TCRs that are not triggered), *n* is the number of TCRs present in the close contact and P_s is the probability that any given TCR remains in the CCZ for t_{min} >2 s. For example, using the predicted physiological size of the CCZ of $r = 0.22\,\mu m$ (Sage et al., 2012), $T_m = 100\,\mu m^{-2}$, $D = 0.05\,\mu m^2/s$ and $t_f = 180\,s$, the triggering probability is just $2 * 10^{-4}$, which suggests that ligand-independent triggering is unlikely in this case.

Equations 2.1-2.6 can be used to predict the residence time and probability that unbound TCRs stay longer than t_{min} seconds inside the CCZ, giving single-exponential distributions of the residence time in the CCZ. However, allowing TCRs to bind pMHC ($K > 0$ in eq. 2.1) in the CCZ gives biphasic distributions since two populations exist: (1) a population of unbound TCRs that are freely-diffusing and (2) a population of pMHC-bound TCRs (that cannot diffuse outside the CCZ). We model the time-dependent evolution of these populations using two simple differential equations:

$$\frac{dU}{dt} = -k_{on} \cdot U \cdot \left(M_{pMHC} - B\right) + k_{off} B - \left(\frac{1}{\tau}\right) \cdot U \qquad \text{(Equation 2.7)}$$

$$\frac{dB}{dt} = k_{on} \cdot U \cdot \left(M_{pMHC} - B\right) - k_{off} B \qquad \text{(Equation 2.8)}$$

where U and B are the densities of unbound and bound TCRs, respectively. Unbound TCRs can either bind pMHC (M_{pMHC}) at rate k_{on}, or diffuse out of the CCZ at rate $1/\tau$, where τ is the mean residence time. Bound TCRs dissociate at rate k_{off}. The equations were solved with the initial TCR density of 100 molecules/μm^2 ($U(0) = 100$) and no bound TCRs ($B(0) = 0$), using MATLAB R2014b with the ode15s solver (MathWorks, Inc.). The probability that a TCR remains longer than t_{min} seconds inside the CCZ was calculated as the fraction of the area under the curve, for U after all TCRs have diffused out of the CCZ, covering the "right-hand side" of t_{min}.

Quantification and Statistical analysis

Data were analysed by Graphpad Prism and Origin Lab built-in T-test (unpaired, two tailed), and results were considered significant when $p < 0.05$. Other statistical parameters including the number of replicates, fold-changes, percentages, SEM, SD, number of cells, number of tracks and statistical significance are reported in the figures, figures legends, supplemental table and supplemental data.

bioRxiv preprint doi: https://doi.org/10.1101/109785; this version posted February 19, 2017. The copyright holder for this preprint (which was not certified by peer review) is the author/funder. All rights reserved. No reuse allowed without permission.

References

Burroughs, N. J., Lazic, Z. & van der Merwe, P. A. Ligand detection and discrimination by spatial relocalization: A kinase-phosphatase segregation model of TCR activation. *Biophys. J.* **91,** 1619–29 (2006).

Davis, S. J., Ikemizu, S., Wild, M. K. & van der Merwe, P. A. CD2 and the nature of protein interactions mediating cell-cell recognition. *Immunol. Rev.* **163,** 217–36 (1998).

Davis, S. J. & van der Merwe, P. A. The kinetic-segregation model: TCR triggering and beyond. *Nat. Immunol.* **7,** 803–9 (2006).

Edelstein A., Amodaj N., Hoover K., Vale R., Stuurman N. Computer control of microscopes using µManager. Curr Protoc Mol Biol **14,** 1–14 (2010).

Fritzsche M., Fernandes RA., Colin-York H., Santos AM., Lee SF., Lagerholm BC., Davis SJ., Eggeling C.
CalQuo: automated, simultaneous single-cell and population-level quantification of global intracellular Ca2+ responses. Sci. Rep. **5**, (2013).

Jansson, A. A mathematical framework for analyzing T cell receptor scanning of peptides. *Biophys. J.* **99,** 2717–25 (2010).

McKeithan, T. W. Kinetic proofreading in T-cell receptor signal transduction. *Proc. Natl. Acad. Sci. U. S. A.* **92,** 5042–6 (1995)

Miller, M.J., Hejazi, A.S., Wei, S.H., Cahalan, M.D., Parker, I. T cell repertoire scanning is promoted by dynamic dendritic cell behavior and random T cell motility in the lymph node. Proc Natl Acad Sci U S A. **101**, 998-1003 (2004).

Ptacin J. L., Lee S. F., Garner E.C., Toro E., Eckart M., Comolli L.R., Moerner W.E., Shapiro L. A spindle-like apparatus guides bacterial chromosome segregation. *Nat Cell Biol.* **12,** 791-8 (2010).

Rosenbluth, M.J., Lam, W.A., Fletcher, D.A. Force microscopy of nonadherent cells: a comparison of leukemia cell deformability. *Biophys J* **90,** 2994–3003 (2006).

Schneider, C. A.; Rasband, W. S. & Eliceiri, K. W., NIH Image to ImageJ: 25 years of image analysis, *Nature methods* **9,** 671-5 (2012).

Stoll, S., Delon, J., Brotz, T.M., Germain, R.N. Dynamic imaging of T cell-dendritic cell interactions in lymph nodes. Science. **296,** 1873-6 (2002).

Vogelsang, J., Cordes, T., Forthmann, C., Steinhauer, C., Tinnefeld, P., Controlling the fluorescence of ordinary oxazine dyes for single-molecule switching and superresolution microscopy. *Proc. Natl. Acad. Sci. U. S. A.* **106,** 8107–12 (2009)

Weaver, D. L. Diffusion-mediated localization on membrane surfaces. *Biophys J* **41,** 81 (1983).

Weimann L., Ganzinger K.A., McColl J., Irvine K.L., Davis S.J., Gay N.J., Bryant C.E., Klenerman D. (2013) A Quantitative Comparison of Single-Dye Tracking Analysis Tools Using Monte Carlo Simulations. PLoS One **8,** e64287.

Wofsy, C., Coombs, D. & Goldstein, B. Calculations show substantial serial engagement of T cell receptors. *Biophys. J.* **80,** 606–12 (2001).

bioRxiv preprint doi: https://doi.org/10.1101/109785; this version posted February 19, 2017. The copyright holder for this preprint (which was not certified by peer review) is the author/funder. All rights reserved. No reuse allowed without permission.

II. Supplementary Tables

Table S1

Quantitative characterization of the T cell – surface (glass) contacts and the organization of key signaling proteins within these areas based on fluorescence microscopy data at single-molecule resolution

Values from the data presented in **Figure 1**. Measurable contacts are defined as spatially isolated zones of CD45 segregation that are larger than the diffraction limit. *Trajectories were classified as "confined" if they could be mapped exclusively onto the inner area of a zone (denoted by "1" in the binary representation of the zones, cf. **Figure 1 B-D**). †Quoted is the fraction of a molecule's density "in" the contact over its total density in the visible area of the cell. ^mouse Lck mutated to eliminate CD4 binding (Chang et al. 2016)

	# cells	# zones analysed	Average zone area [μm^2]	Average zone radius [µm]	# molecules tracked	Confined/total molecules (fraction†)
CD45	24	113	0.9759±0.0851	0.2±0.4	569	18/569 (0.032±0.007)
Lck (mm)	15	50	1.2988± 0.1695	0.2±0.4	318	106/318 (0.333±0.026)
hLck	40	69	0.5617± 0.0441	0.1±0.3	434	25/434 (0.057±0.011)
TCR	30	83	0.5685± 0.0723	0.1±0.3	206	11/206 (0.053±0.015)
HA-CD45	20	73	1.0389± 0.0929	0.2±0.4	407	56/407 (0.138±0.018)

bioRxiv preprint doi: https://doi.org/10.1101/109785; this version posted February 19, 2017. The copyright holder for this preprint (which was not certified by peer review) is the author/funder. All rights reserved. No reuse allowed without permission.

Table S2

Quantitative characterization of close contacts between T cells and rCD2-SLB and the organization of key signaling proteins within these areas based on fluorescence microscopy data at single-molecule resolution

Values from the data presented in **Figure 1**. The automated procedure used to dissect the images and define the cell-SLB contacts are described in the Online Methods. *Trajectories were classified as "confined" if they could be mapped exclusively onto the inner area of a zone (denoted by "1" in the binary representation of the zones, cf. Figure **1 E-G**, *right panels*). †Quoted is the fraction of a molecule's density "in" the contact over its total density in the visible area of the cell.

	# cells	Average zone area [μm^2]	Average zone radius [μm]	Confined*/total molecules	Ratio of density of confined molecules and total density†
CD45	39	25±20	1.3±2.5	65/969	0.18
Lck	16	16±21	1.5±1.7	234/1527	0.46
TCR	16	13±12	1.7±1.2	48/375	0.37

Table S3

Parameters used for Model 1 to derive the analysis shown in Figure 3 and 4.

	Fig. 3B	Fig. 3C	Fig. 3D	Fig. 3E	Fig. 4A	Fig. 4B	Fig. 4C	Fig. 4D	Fig. 4E	Fig 4F
cell surface area [μm²]						415[7]				
close contact radius [μm]		*variable*		*variable*[1]	0.22[5]/ 0.44[5]		0.22[5]		*variable*	0.22[5]
number of close contacts					1					
# TCR copies/cell	41,500[2]	15,000[2]				41,500[2]				
# CD45 copies/cell					200,000[5]					
# Lck copies/cell					40,000[5]					
fraction of TCR segregation		0.63[2,3]/ 0.96[2,4]								
CD45:Lck ratio		2.5:1[2]		*variable*			2.5:1[2]			
TCR diffusion [μm²/s]	0.05[3]	0.027[4]/ 0.05[3]	0.027[4]/0.05[3]	0.05[3]			0.05			
k_{on} (pMHC)		NA				0.1		*variable*	0.1	0.1
agonist pMHC [molecules/μm²] / k_{off}		NA			NA	30 / 1	30 / *variable*	30 / *variable*	30 / 1	30 / 1
non-agonist pMHC [molecules/μm²] / k_{off}		NA			NA	300 / 50	*300 / variable*	300 / *variable*	NA	30 / *variable*
t_{min} [s]	NA	2[5]		2[5]/20			2[5]			
Fraction of triggered TCRs	NA	*result*	NA	0.5[6]			NA			
T cell-APC contact duration		120s			*variable*		*variable*	120s	*variable*	120s

[1]growth rate, *g* [um/s];
[2]experimentally determined for CD4 T cells isolated from PBMCs;
[3]SLB;
[4]IgG-coated glass;
[5]referenced from literature, *c.f.* main text for details;
[6]arbitrary value to plot linear relationship;
[7] (Weaver., 1983).

bioRxiv preprint doi: https://doi.org/10.1101/109785; this version posted February 19, 2017. The copyright holder for this preprint (which was not certified by peer review) is the author/funder. All rights reserved. No reuse allowed without permission.

Table S4

Parameters used for Model 2 to derive the analysis shown in SI Figure 6 and 7

	SI Fig 6A	SI Fig. 6B	SI Fig. 7A	SI Fig. 7B	SI Fig. 7C	SI Fig. 7D
cell radius [μm]	5.75[7]			5.75[7]		
close contact radius [μm]	*variable*		0.22[5]	0.22[5]/0.33[5]	*variable*	0.22[5]
number of close contacts	1			1		
# TCR copies/cell	15,000[2]			15,000[2]		
# CD45 copies/cell	200,000[5]			200,000[5]		
# Lck copies/cell	40,000[5]			40,000[5]		
fraction of TCR segregation	0.63[2,3]/0.96[2,4]			0.63[2,3]/0.96[2,4]		
CD45:Lck ratio	2.5:1[2]			2.5:1[2]		
TCR diffusion [μm^2/s]	0.027[4]/0.054[3]	0.027[4]/0.054[3]		0.05		
k_{on} (pMHC)	NA			0.01		*variable*
agonist pMHC [molecules/μm^2] / k_{off}	NA		30 / 0.5	NA	30 / 0.5	30 / *variable*
non-agonist pMHC [molecules/μm^2] / k_{off}	NA		300 / 10	NA	NA	300 / *variable*
t_{min} [s]	2[5]					
Fraction of triggered TCRs	*variable*		N.A.			
T cell-APC contact duration	NA		*variable*		*variable*	120s
Triggering probability	NA		*variable*		NA	*variable*

[1]growth rate, *g* [μm/s]
[2]experimentally determined;
[3]SLB; [4]IgG-coated glass
[5]referenced from literature, *c.f.* main text and supplementary for details
[7] Rosenbluth et al., 2006.

bioRxiv preprint doi: https://doi.org/10.1101/109785; this version posted February 19, 2017. The copyright holder for this preprint (which was not certified by peer review) is the author/funder. All rights reserved. No reuse allowed without permission.

bioRxiv preprint doi: https://doi.org/10.1101/109785; this version posted February 19, 2017. The copyright holder for this preprint (which was not certified by peer review) is the author/funder. All rights reserved. No reuse allowed without permission.

III. Supplementary Figures

Figure S1

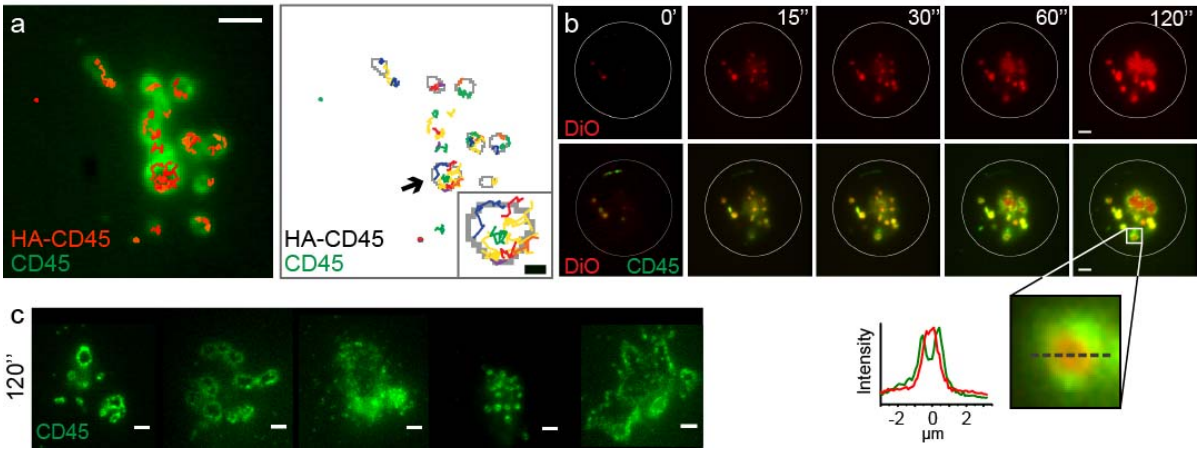

Analysis of the distribution of molecules at close-contacts between T cells and glass surfaces by TIRF microscopy and single-particle tracking. (**a**) Distribution of a variant of CD45 with an ECD comprising a 9-residue hemagglutinin tag and a C-terminal Halo-tag (HA-CD45-Halo) in Jurkat T-cell -glass contacts (CD45 labeled with Alexa Fluor 568-tagged Gap 8.3 Fab (green), HA-CD45-Halo labeled with TMR). (**b**) Evolution of close-contact diameter over time from TIRFM time lapses of close-contacts showing that the contacts mostly merge during the first 2 minutes of cell-surface contact. (**c**) Representative images (n_{cells} =20) of CD45 distribution (Alexa Fluor 568-tagged Gap 8.3 Fab (green)) in Jurkat T cell contacts with IgG-coated glass surfaces 2 minutes after the cells landing on the surface, showing a large heterogeneity in close contact size but invariable CD45 exclusion from the close contacts. All scale bars are 2 µm.

bioRxiv preprint doi: https://doi.org/10.1101/109785; this version posted February 19, 2017. The copyright holder for this preprint (which was not certified by peer review) is the author/funder. All rights reserved. No reuse allowed without permission.

Figure S2

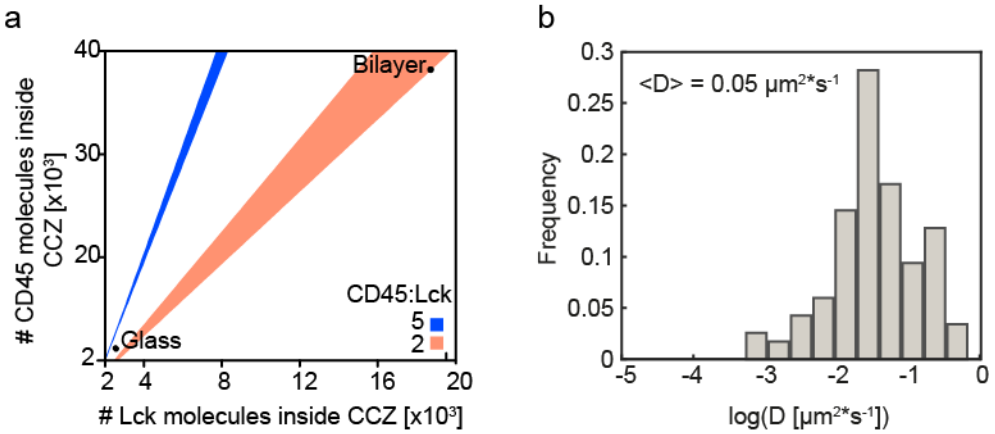

Quantitative analysis of CD45 and Lck density and TCR diffusion at close-contacts between T cells and glass surfaces by single-particle tracking. (**a**) Graphical depiction of the parameter space (numbers of CD45 and Lck molecules in the T cell membrane) covered by different CD45:Lck ratios (±0.25; **b**). Histogram of diffusion coefficients D obtained from linear fits (5 points, interval 35ms) to mean-square displacement (MSD) of single TCRs (data presented in **Figure 1D**). Trajectories for CD45 and Lck were analyzed analogously to calculate their respective diffusion coefficients in **Figure 1H**. The diffusion coefficient quoted in the table of **Figure 1H** is the mean (<D>) and the error the s.d. of the distribution of D.

bioRxiv preprint doi: https://doi.org/10.1101/109785; this version posted February 19, 2017. The copyright holder for this preprint (which was not certified by peer review) is the author/funder. All rights reserved. No reuse allowed without permission.

Figure S3

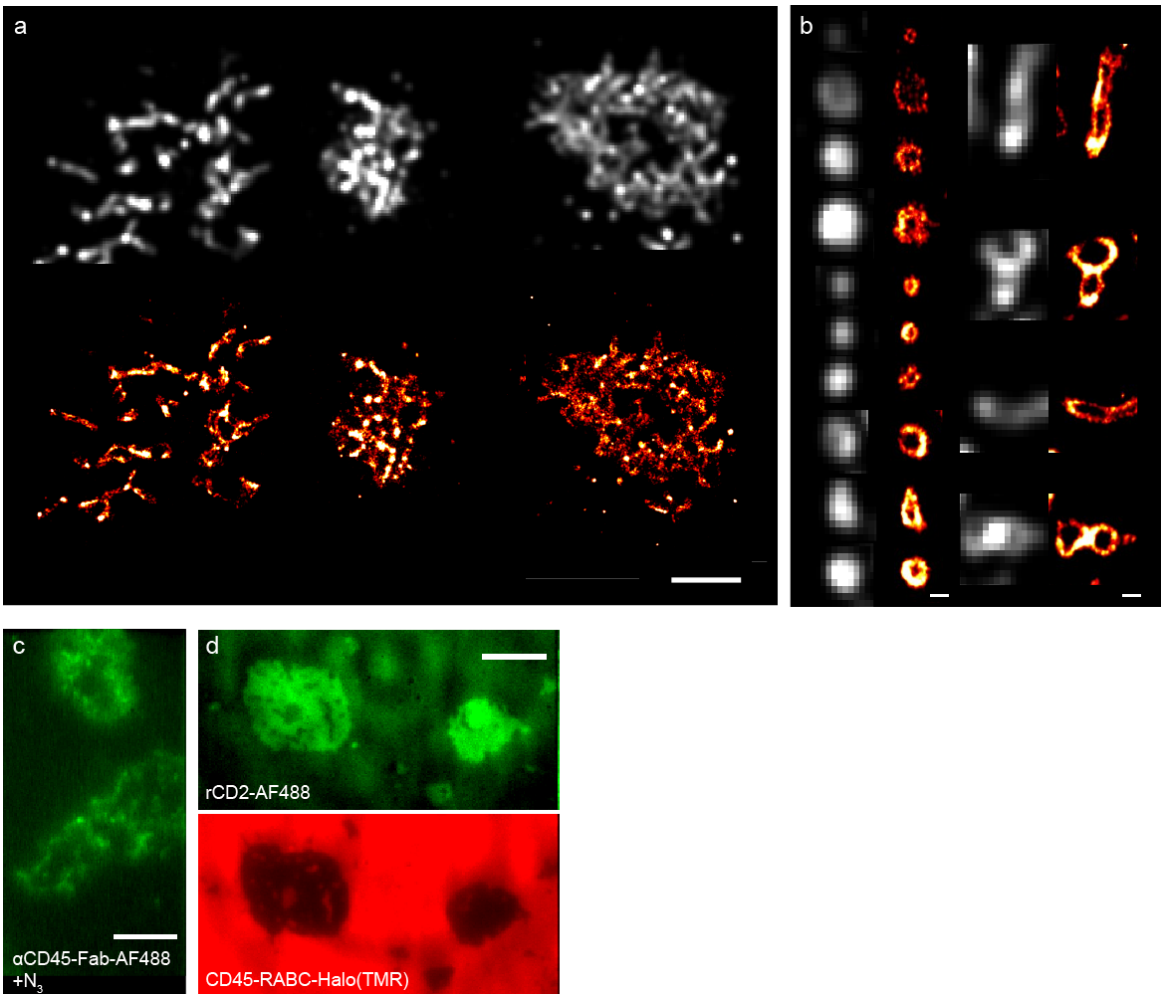

CD45 segregates from close-contacts between T cells and glass surfaces at sub-µm length scales in a process that is independent of ATP and other cell-specific components. Distribution of CD45 at close-contacts between three T cells and IgG-coated glass as seen by super-resolution (dStorm) imaging; representative field of view (**a**) and (**b**) galley of 20 individual close-contacts sampled across > 5 cells. (**c**) CD45 distribution in contacts of N_3-treated, ATP-depleted CD48+ Jurkat T-cells with SLBs containing rCD2 SLBs (Alexa Fluor 568-tagged Gap 8.3 Fab; green). (**d**) The spatial organization of rCD2 (Alexa Fluor 488-tagged, green, 1000 molecules/µm^2, top) and CD45-RABC-Halo (TMR labeled, red, bottom) in contacts of CD48+ Jurkat T-cells and SLBs containing rCD2 and CD45-RABC-Halo (4:1) 8 minutes after cells landing on the SLB. Scale bars (**a**) 3 µm, (**b**) 200 nm, (**c,d**) 5 µm.

bioRxiv preprint doi: https://doi.org/10.1101/109785; this version posted February 19, 2017. The copyright holder for this preprint (which was not certified by peer review) is the author/funder. All rights reserved. No reuse allowed without permission.

Figure S4

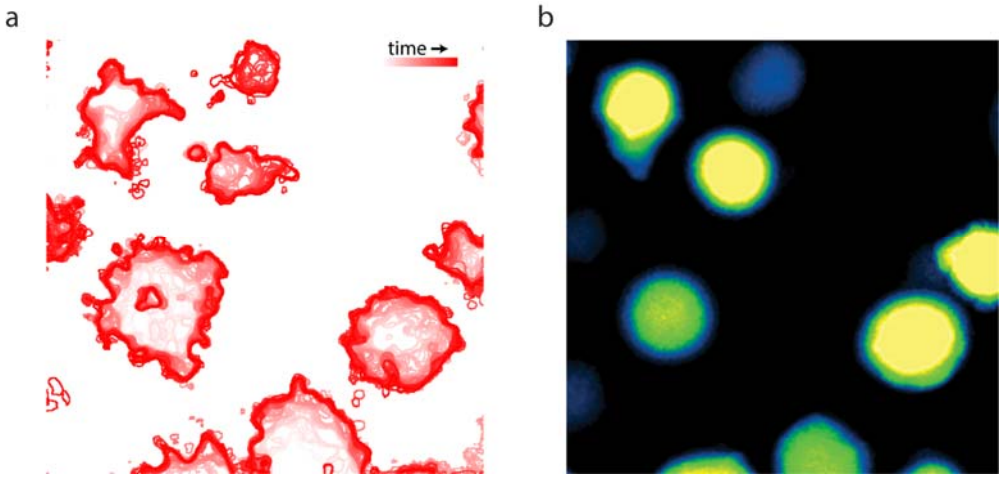

Simultaneous detection of close contact formation and calcium release on Jurkat T cells interacting with IgG-coated glass surfaces. (**a**) Temporal color-coded contour of the outer edge of close contacts formed by T cells upon interaction with IgG-coated glass surfaces using IRM (**b**) Temporal color-coded intensity of Fluo-4 fluorescence for the same cells shown in (**a**). IRM and Fluo-4 fluorescence intensity were acquired simultaneously with 488 nm excitation laser. The temporal color-coded images correspond to 66 frames acquired at ~6 frames/s.

bioRxiv preprint doi: https://doi.org/10.1101/109785; this version posted February 19, 2017. The copyright holder for this preprint (which was not certified by peer review) is the author/funder. All rights reserved. No reuse allowed without permission.

Figure S5

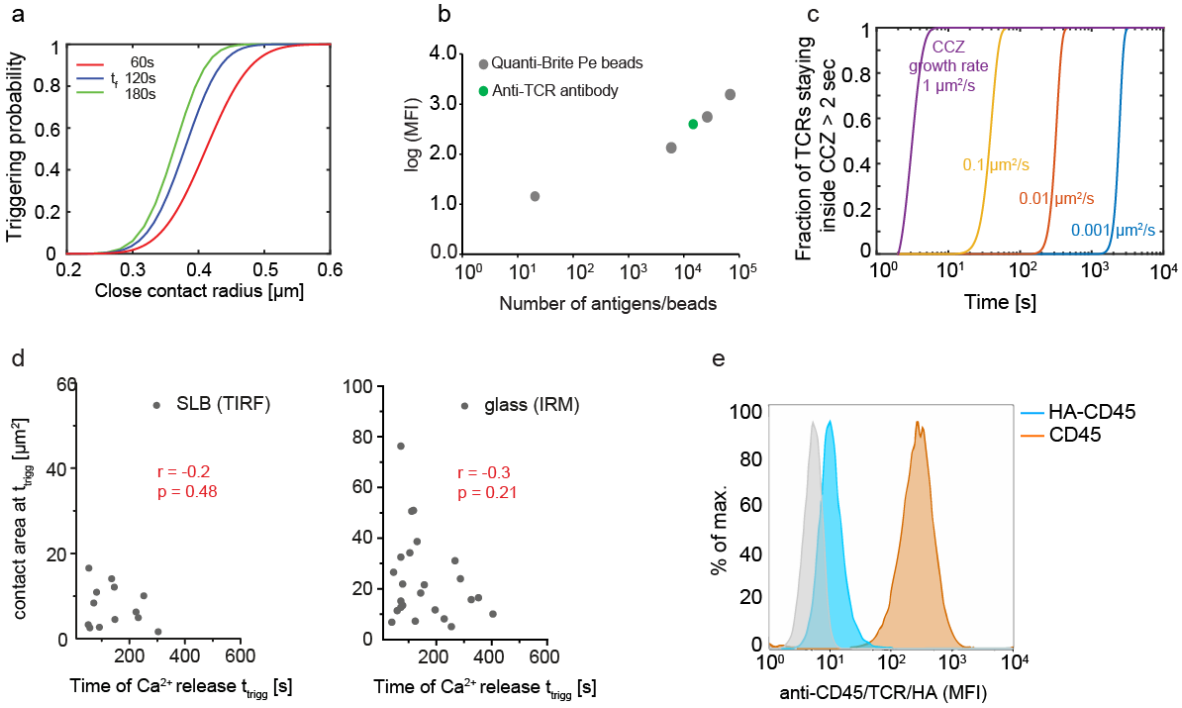

Dependence of the mathematical description of the KS model for TCR triggering on various parameters and testing the validity of assumptions made (Model 1). (**a**) Probability that a TCR is triggered (*i.e.* a TCR remains inside the CCZ for longer than 2 seconds) as a function of close contact radius for different times of cell-cell interaction (t_f) and thus persistence of the CCZ. (**b**) Quantification of the number of TCR per cell measuring mean fluorescence intensity of anti-TCR PE labeled antibody by FACS and QuantiBrite PE beads. (**c**) Fraction of triggered TCRs as a function of time and different growth rates (t_{min} = 2 s, D = 0.05 µm^2/s, g = 0.01 – 10 µm^2/s). (**d**) The size of the contact area at t_{trigg} is approximately constant for contacts formed on SLBs and glass; *i.e.* the slope of contact area at t_{trigg} over t_{trigg} is not significantly different from 0 (ANOVA on linear regression, p =0.48 and 0.21, respectively). Total numbers of cells analyzed were $n_{(glass,\ IRM)}$ = 24 and $n_{(SLB,\ TIRF)}$ = 17 from n > 5 samples. (**e**) Mean fluorescence intensity of anti-HA (clone HA-7, Sigma, HA-7) or anti-CD45 (Gap 8.3) antibodies on Jurkat T cells transduced with HA-CD45. In grey, anti-HA staining of untransduced Jurkat T cells.

bioRxiv preprint doi: https://doi.org/10.1101/109785; this version posted February 19, 2017. The copyright holder for this preprint (which was not certified by peer review) is the author/funder. All rights reserved. No reuse allowed without permission.

Figure S6

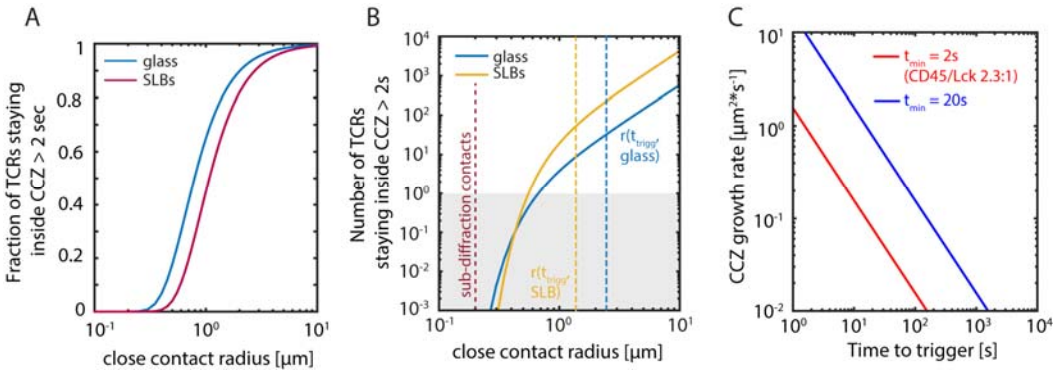

Ligand-independent TCR triggering depends on close-contact area and duration (Model 2). (**A**) Fraction of TCRs that remains inside the close contact for longer than 2 seconds as a function of the radius of the contact area (equation 2.2; all parameters used can be found in **Table S4**). (**B**) Total number of TCRs that remain inside the close contact for longer than 2 seconds, considering the estimates shown in (**A**), the density of TCRs in Jurkat T cells, the segregation of TCR from close contacts and the mean residence time inside close contacts for cells interacting with IgG-coated glass surfaces (blue line) or rCD2-SLBs (yellow line). (**C**) Dependence of the time taken to TCR triggering as a function of growth rate of close contact zones (as shown in equation 2.4: t_{min} = 2, D = 0.05, p_{min} = 0.2; p_{min} is an arbitrary number between 0 and 1 and does not affect the inverse relationship here shown). For a t_{min} = 20 (higher CD45:Lck ratio; blue line) triggering takes on average 10x longer at a given close contact growth rate *g* than for a CD45:Lck ratio of 2.3:1 (red line).

bioRxiv preprint doi: https://doi.org/10.1101/109785; this version posted February 19, 2017. The copyright holder for this preprint (which was not certified by peer review) is the author/funder. All rights reserved. No reuse allowed without permission.

Figure S7

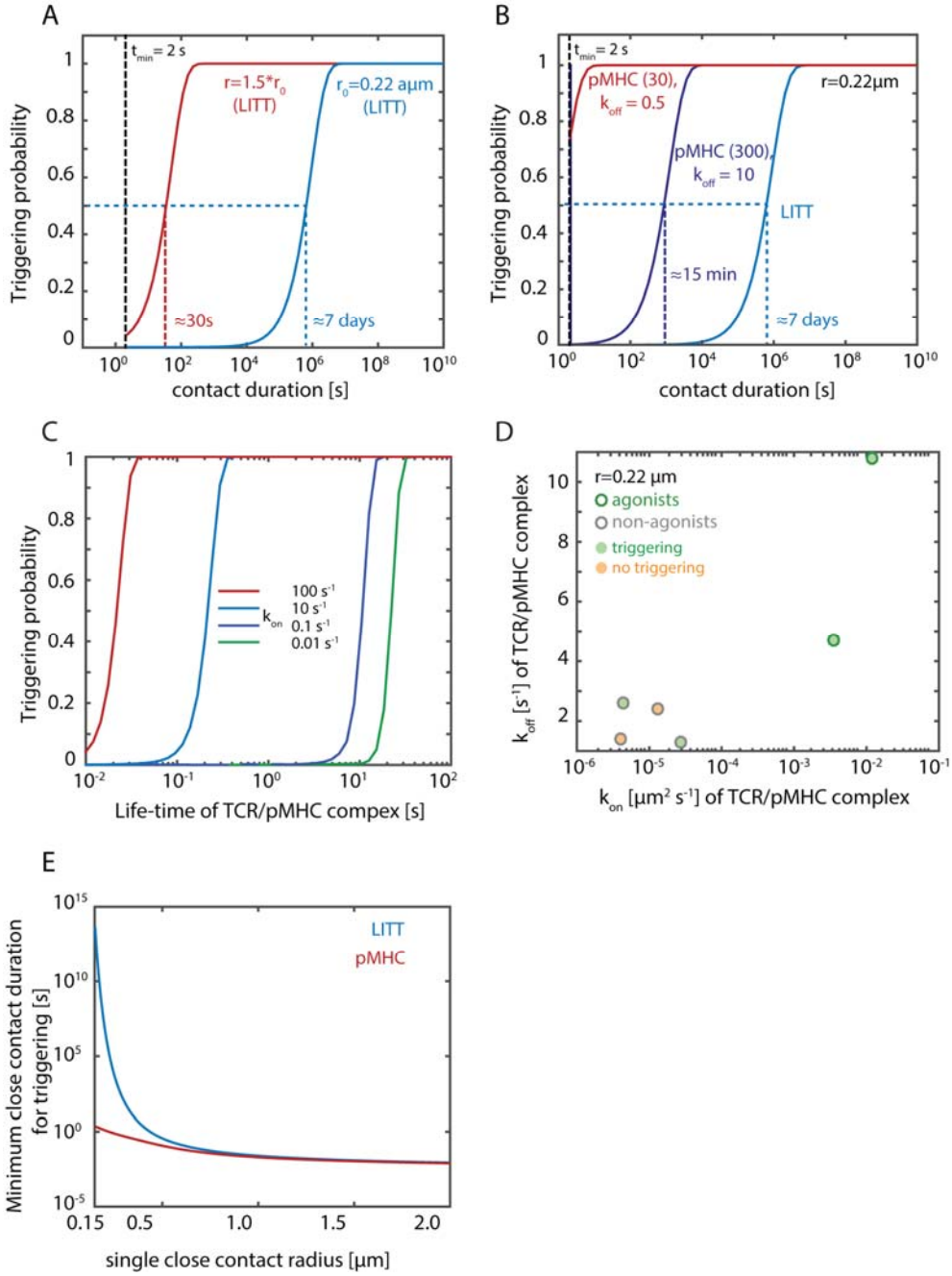

TCR signalling depends on ligand-binding and LIT may play a role in signalling amplification (Model 2). (**A**) Probability of triggering of at least one TCR as a function of contact duration. For a close contact similar to the reported size *in vivo* (0.22 μm) and for a

bioRxiv preprint doi: https://doi.org/10.1101/109785; this version posted February 19, 2017. The copyright holder for this preprint (which was not certified by peer review) is the author/funder. All rights reserved. No reuse allowed without permission.

larger close contact (0.32 μm; ligand independent TCR triggering). (**B**) Probability of triggering of at least one TCR as a function of contact duration in the presence and absence of agonist pMHC with a low k_{off} (k_{off} = 0.5, 30 pMHC molecules/μm^2) and of pMHC with a larger k_{off} at higher pMHC densities (k_{off} = 10, 300 pMHC molecules/μm^2) for a close contact a radius of 0.22 μm. (**C**) Triggering probability as a function of pMHC-TCR life-time ($1/k_{off}$) for pMHC-TCR complexes of varying association rates (k_{on}). (**D**) Prediction of triggering behavior for pMHC-TCR pairs with published 2D k_{on} and k_{off} values (Huang et al.) and known classification (agonist/non-agonist); the pMHC-TCR interaction is assumed to trigger cell signalling if the predicted contact time required for at least one TCR triggering event occurs in less than 120 s for a single close contact of radius 0.22 μm. (**E**) Effect of the close contact radius on the contact time required for T cell triggering in the presence or absence (LITT) of agonist pMHC (k_{off} = 0.5, 30 pMHC molecules/μm^2).

bioRxiv preprint doi: https://doi.org/10.1101/109785; this version posted February 19, 2017. The copyright holder for this preprint (which was not certified by peer review) is the author/funder. All rights reserved. No reuse allowed without permission.

Figure S8

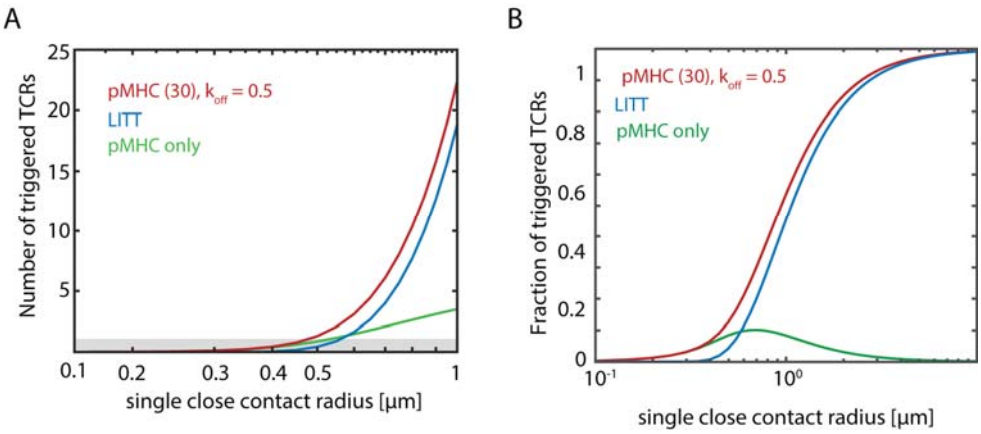

Number and fraction of triggered TCRs for a single close contact radius in both the presence and absence of agonist pMHC. (**A**) Number and (**B**) fraction of triggered TCRs in the absence (blue curve; LIT) or presence (red curve) of agonist pMHC with a low k_{off} (k_{off} = 0.5, 30 pMHC molecules/μm^2. In the presence of pMHC, ligand-independent TCR triggering also contributes to the total number of triggered TCRs (red curve). For larger close contacts, the number of ligand-independent triggered TCRs is increasingly higher in proportion to pMHC driven triggering as shown by the number of TCRs triggered by agonist-binding alone, as determined by the difference between the pMHC and LIT curves (green line).

bioRxiv preprint doi: https://doi.org/10.1101/109785; this version posted February 19, 2017. The copyright holder for this preprint (which was not certified by peer review) is the author/funder. All rights reserved. No reuse allowed without permission.

Figure S9

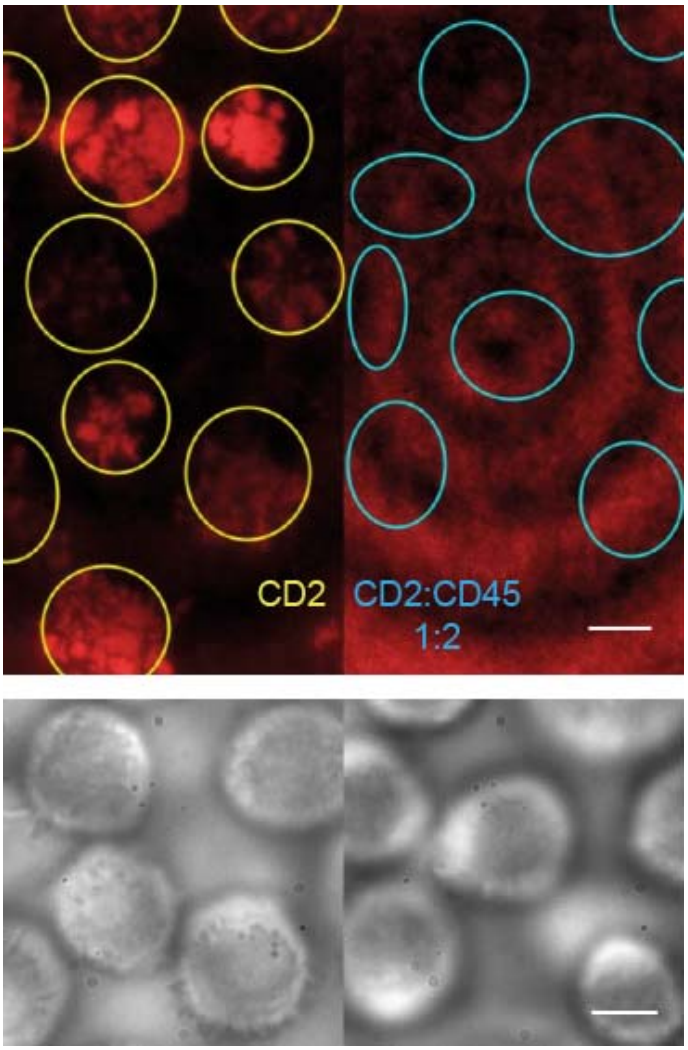

The presence of SLB-bound CD45-RABC ectodomain inhibits contact formation of CD48+ Jurkat T-cells with rCD2 SLBs. The spatial organization of rCD2 (Alexa Fluor 647-tagged, red) during contact of Jurkat T-cells expressing a transmembrane-anchored, non-signaling, T92A-mutated form of CD48 ($CD48^+$) and SLBs containing rCD2 (*top, left,* 240 molecules/μm^2) or rCD2 and CD45-RABC (1:2, *top, right,* 250 molecules/μm^2 of rCD2) 8 minutes after cells landing on the SLB. The position of cells is marked in yellow and cyan (cf. *bright field images, bottom*). All scale bars are 5 µm.

bioRxiv preprint doi: https://doi.org/10.1101/109785; this version posted February 19, 2017. The copyright holder for this preprint (which was not certified by peer review) is the author/funder. All rights reserved. No reuse allowed without permission.

Supplementary Movies (descriptions)

Movie S1

Single-molecule tracking data (CD45, TCR; IgG-coated glass). Representative movies (raw data) showing single-molecule tracking of key signaling molecules (CD45, *left*, TCR, *right; red*) at close-contacts visualized by high-density labeling of CD45 (*green*). Movies are part of the data presented in **Figure 1**. The movie shows an overlay of the raw data for the CD45 channel (*i.e.* CD45 labeled with Alexa Fluor 488-tagged Gap 8.3 Fab (*green*), averaged over 200 frames) with the single-molecule channel (*i.e. CD45/TCR* labeled with Alexa Fluor 568-tagged Gap 8.3 Fab/HaloTag® TMR, *red*, raw data). The movie is played back in 0.5 x real-time (14 frames per second); scale bar and time are displayed in the movie.

Movie S2

Close contact growth Representative movie (raw data, 20°C) showing the merging of several individual close contacts (visible from ~1′) into one (from ~2′) over time. The movie is played back 8x faster than real-time; scale bar and time are displayed in the movie.

Movie S3

Single-molecule tracking data (CD45; rCD2-SLB). Representative movie (raw data) showing single-molecule tracking of key signalling molecules (CD45, *red*) at close contacts visualized by high-density labeling of CD45 (*green*). Movies are part of the data presented in **Figure 1**. The movie shows an overlay of the raw data for the CD45 channel (*i.e.* CD45 labeled with Alexa Fluor 488-tagged Gap 8.3 Fab, *green*, averaged over 200 frames) with the single-molecule channel (*i.e. CD45* labeled with Alexa Fluor 568-tagged Gap 8.3 fab, *red*). The movie is played back in real-time (29 frames per second, indicated in top left corner); scale bar and time are displayed in the movie.

Movie S4

Ca^{2+} release as measured by change in Fluo-4 fluorescence in Jurkat T-cells forming contacts depleted of CD45 with glass (close-contacts visualized by interference reflection microscopy, IRM). Representative movie (raw data) showing the formation of close-contacts by a Jurkat T-cell landing on IgG coated glass using IRM (*left*) and fluorescence microcospy data for the simultaneous measurement Ca^{2+} release (Fluo-4, 488, *right*). The movie is played back 2-fold faster than real-time (13 frames per second). Scale bar, 5 µm.

Movie S5

Ca^{2+} release as measured by change in Fluo-4 fluorescence in Jurkat T-cells forming contacts depleted of CD45 (labeled) with CD2-containing SLBs. Movie

bioRxiv preprint doi: https://doi.org/10.1101/109785; this version posted February 19, 2017. The copyright holder for this preprint (which was not certified by peer review) is the author/funder. All rights reserved. No reuse allowed without permission.

collage analogous to **Movie S4** for a $CD48^+$ Jurkat T-cell; the movie combines raw data for the CD45 channel (*i.e.* CD45 labeled with Alexa Fluor 568-tagged Gap 8.3 Fab (*red, left*) with a movie of the Fluo-4 channel (*green, right*). The movie is played back 10-fold faster than real-time (5 frames per second). Scale bar, 5 µm.

Movie S6

Ca^{2+} release as measured by change in Fluo-4 fluorescence in J.RT3-T3.5 T-cells forming contacts depleted of CD45 (labeled) with CD2-containing SLBs. Movie collage analogous to **Movie S5** for a J.RT3-T3.5 T-cell). The movie is played back 10-fold faster than real-time (5 frames per second). Scale bar, 5 µm.

Movie S7

Animation of the changes in the TCR probability density across a growing close contact over time corresponding to the modelling shown in Figure 3E with g = 0.1 $\mu m^2/s$. Probability of occupation is plotted on the z-axis, the 'time' given in the title is the time post initial contact and the 'remaining mass' refers to the probability that the TCR is still found within the close contact.

Movie S8

CD45-RABC largely prevents formation of CD2-mediated close-contacts by Jurkat T-cells (CD48+) with CD2- and CD45RABC-containing SLBs. Representative movie showing that few CD48+ Jurkat T-cells form stable cell-bilayer contacts (marked by rCD2 accumulation) with rCD2- and CD45RABC-Halo containing SLB (rCD2:CD45RABC-Halo 1:2). The movie shows an xy-scan across an SLB whereby raw data for the CD2 channel (i.e. SLB contains Alexa Fluor 647-tagged CD2, read-out for CCZ formation) are interleaved with bright field images of the same sample showing the location of the T cells. Scale bar, 5 µm.

Movie S9

CD45-RABC spontaneously segregates from CD2-mediated close-contacts formed by Jurkat T-cells (CD48+) with CD2- and CD45RABC-containing SLBs. Representative movie showing simultaneous rCD2 accumulation and segregation of CD45RABC-Halo from stable cell-bilayer contacts of CD48+ Jurkat T-cells interacting with a rCD2- and CD45RABC-Halo containing SLB (rCD2:CD45RABC-Halo 4:1). The movie combines raw data for the CD2 channel (i.e. SLB contains Alexa Fluor 488-tagged CD2 (green, left) with a simultaneously-acquired movie of the CD45RABC-Halo channel (TMR, red, right). The movie is played back 10-fold faster than real-time (5 frames per second). Scale bar, 5 µm.

A

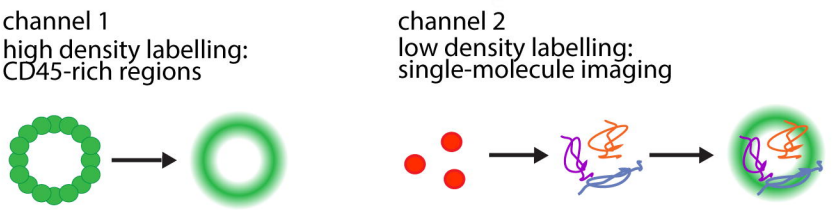

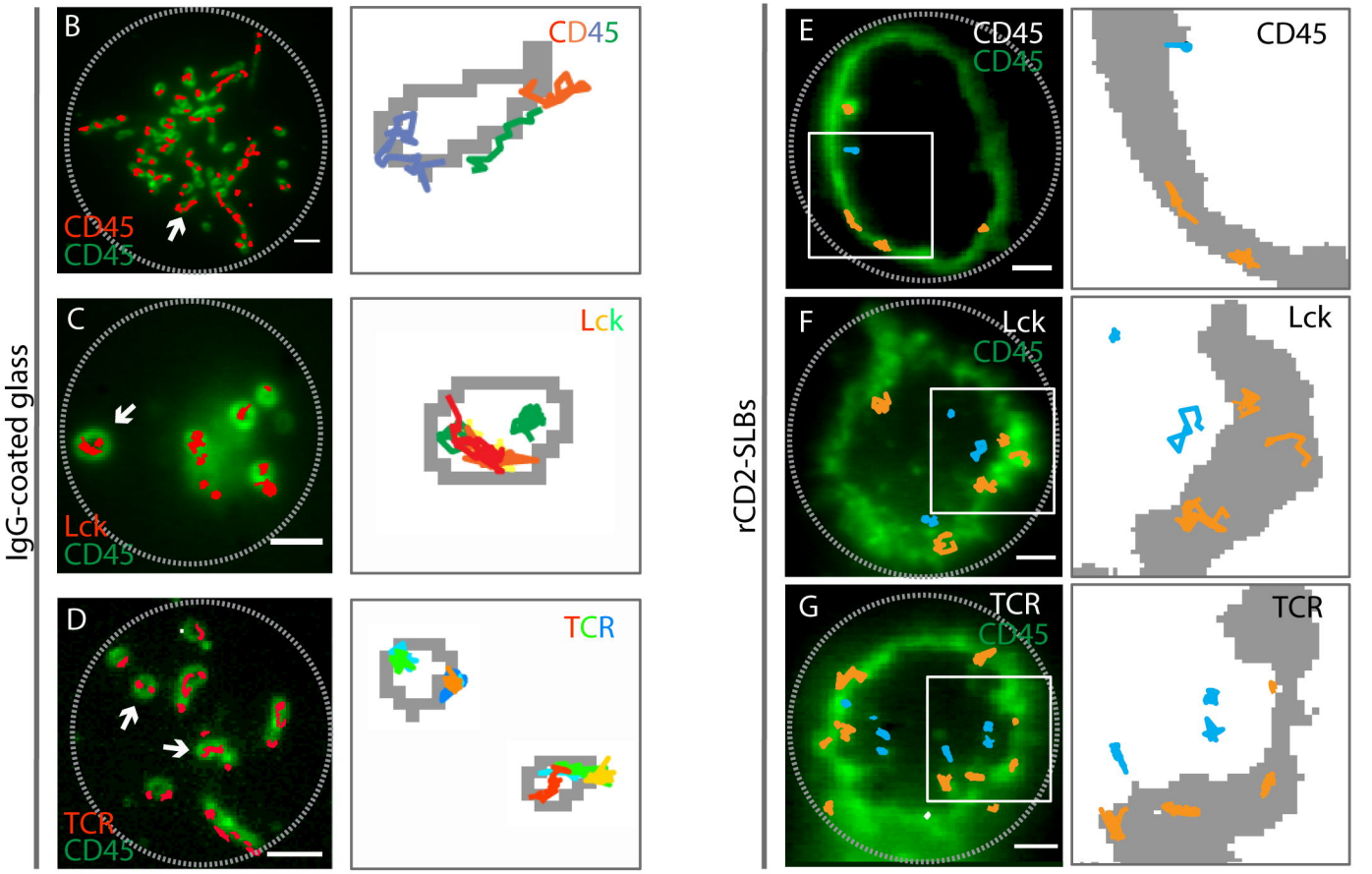

H

		Confined*/ total densities†	Diffusion Coefficient [μm²/s] "inside"	"outside"
IgG-coated glass	CD45	0.032±0.007		
	Lck (mm)	0.333±0.026		
	Lck (wt)	0.057±0.011		
	TCR- β	0.053±0.015	0.027±0.028	
	HA-CD45	0.138±0.018		
rCD2-SLBs	CD45	0.125±0.026		0.113±0.179
	Lck (wt)	0.556±0.067	0.151±0.294	0.104±0.185
	TCR-β	0.399±0.055	0.054±0.107	0.050±0.074

Measurable contacts are defined as spatially isolated zones of CD45 segregation that are larger than the diffraction limit.*Trajectories were classified a "confined" if they could be mapped exclusively onto the inner area of a zone (denoted wtih a gray boundary in the binary representation of the zones in panels b-h); †Quoted is the fraction of trajectory densities rather than numbers.

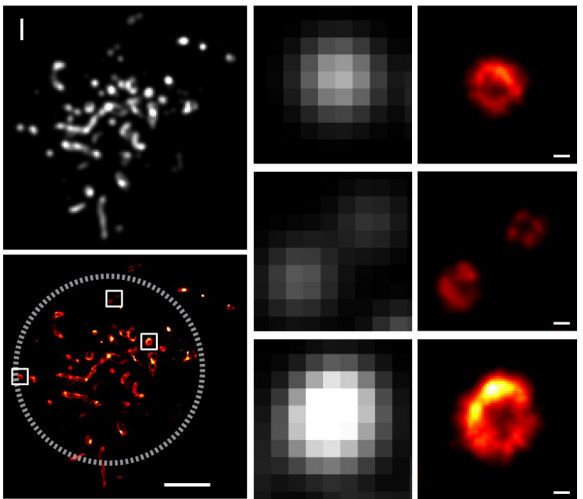

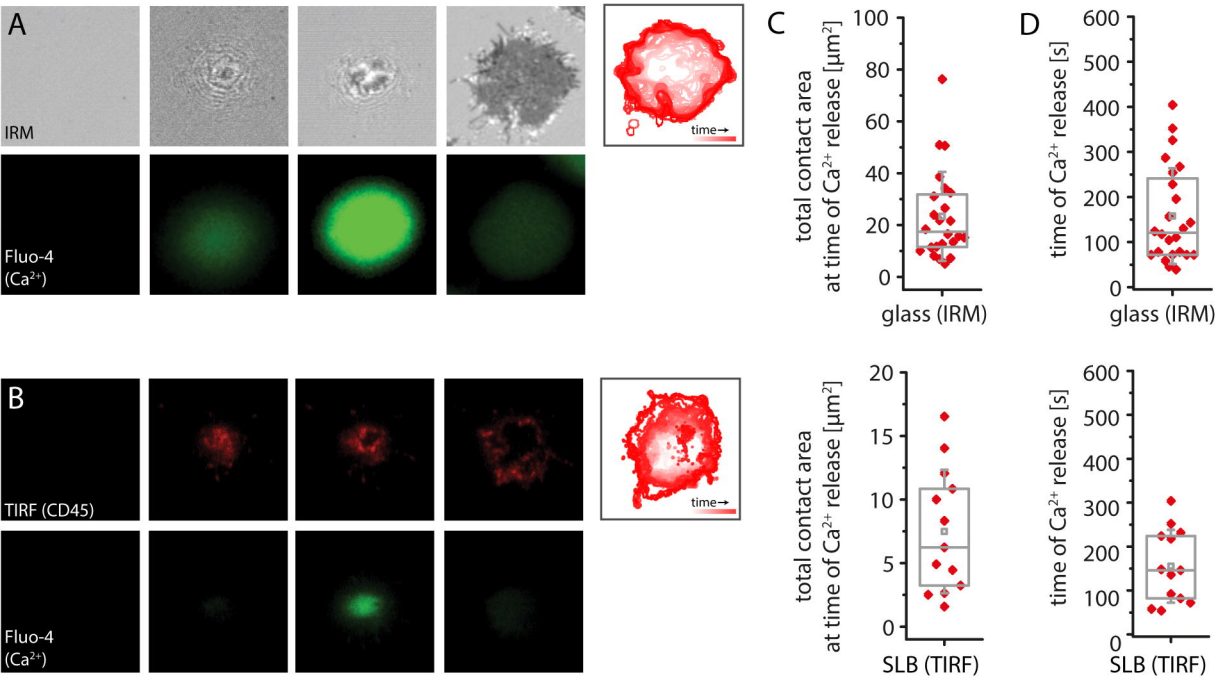
A
IRM
Fluo-4
(Ca2+)
time→
B
TIRF (CD45)
Fluo-4
(Ca2+)
time→
C
total contact area
at time of Ca2+ release [µm2]
glass (IRM)
SLB (TIRF)
D
time of Ca2+ release [s]
glass (IRM)
SLB (TIRF)

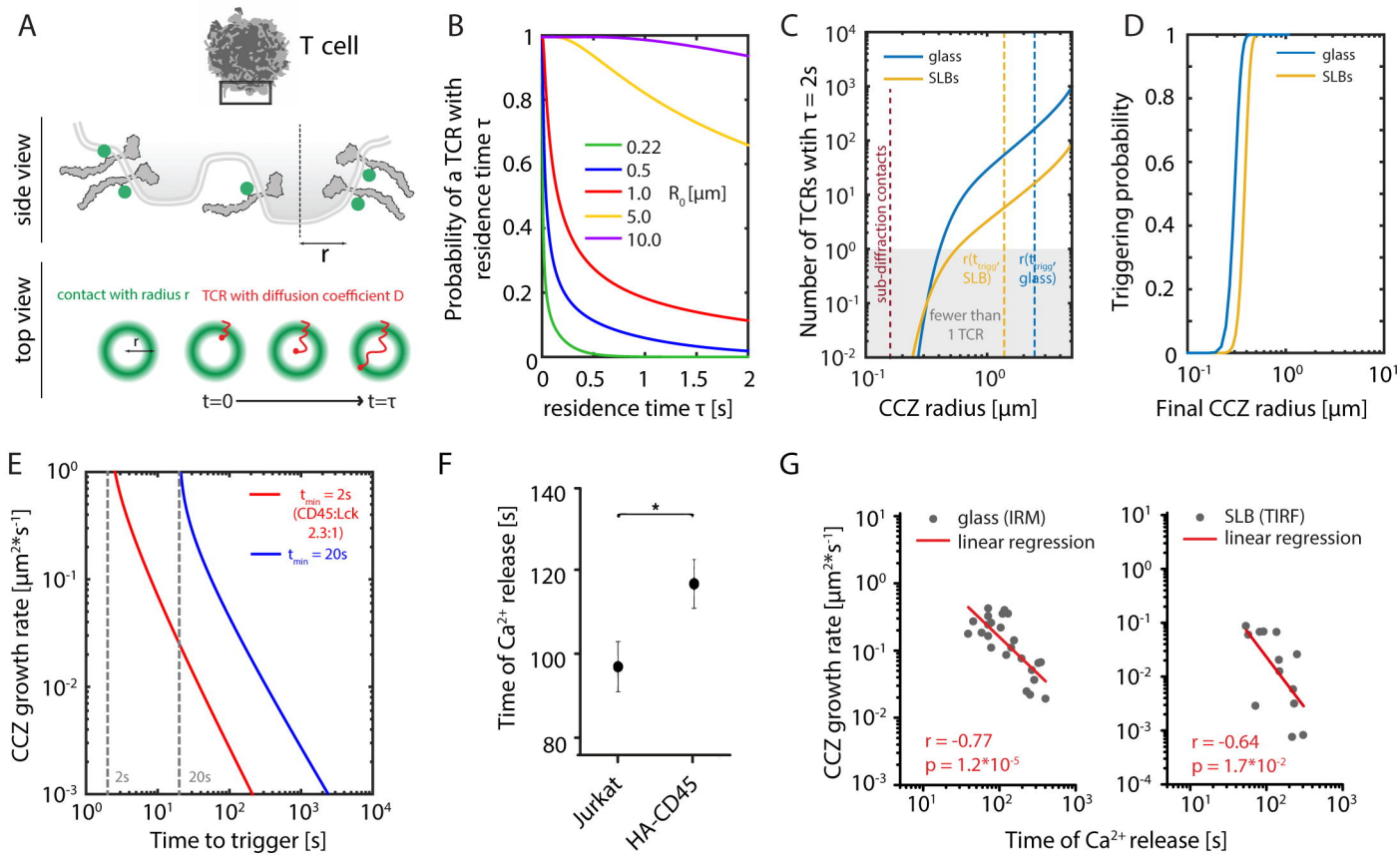
A
T cell
side view
r
top view
contact with radius r
TCR with diffusion coefficient D
t=0
t=τ
B
Probability of a TCR with residence time τ
0.22
0.5
1.0
5.0
10.0
R0 [μm]
residence time τ [s]
C
glass
SLBs
Number of TCRs wtih τ = 2s
sub-diffraction contacts
r(t_trigg, SLB)
r(t_trigg, glass)
fewer than 1 TCR
CCZ radius [μm]
D
glass
SLBs
Triggering probability
Final CCZ radius [μm]
E
t_min = 2s (CD45:Lck 2.3:1)
t_min = 20s
2s
20s
CCZ growth rate [μm²*s⁻¹]
Time to trigger [s]
F
Time of Ca²⁺ release [s]
*
Jurkat
HA-CD45
G
glass (IRM)
linear regression
r = -0.77
p = 1.2*10⁻⁵
SLB (TIRF)
linear regression
r = -0.64
p = 1.7*10⁻²
CCZ growth rate [μm²*s⁻¹]
Time of Ca²⁺ release [s]

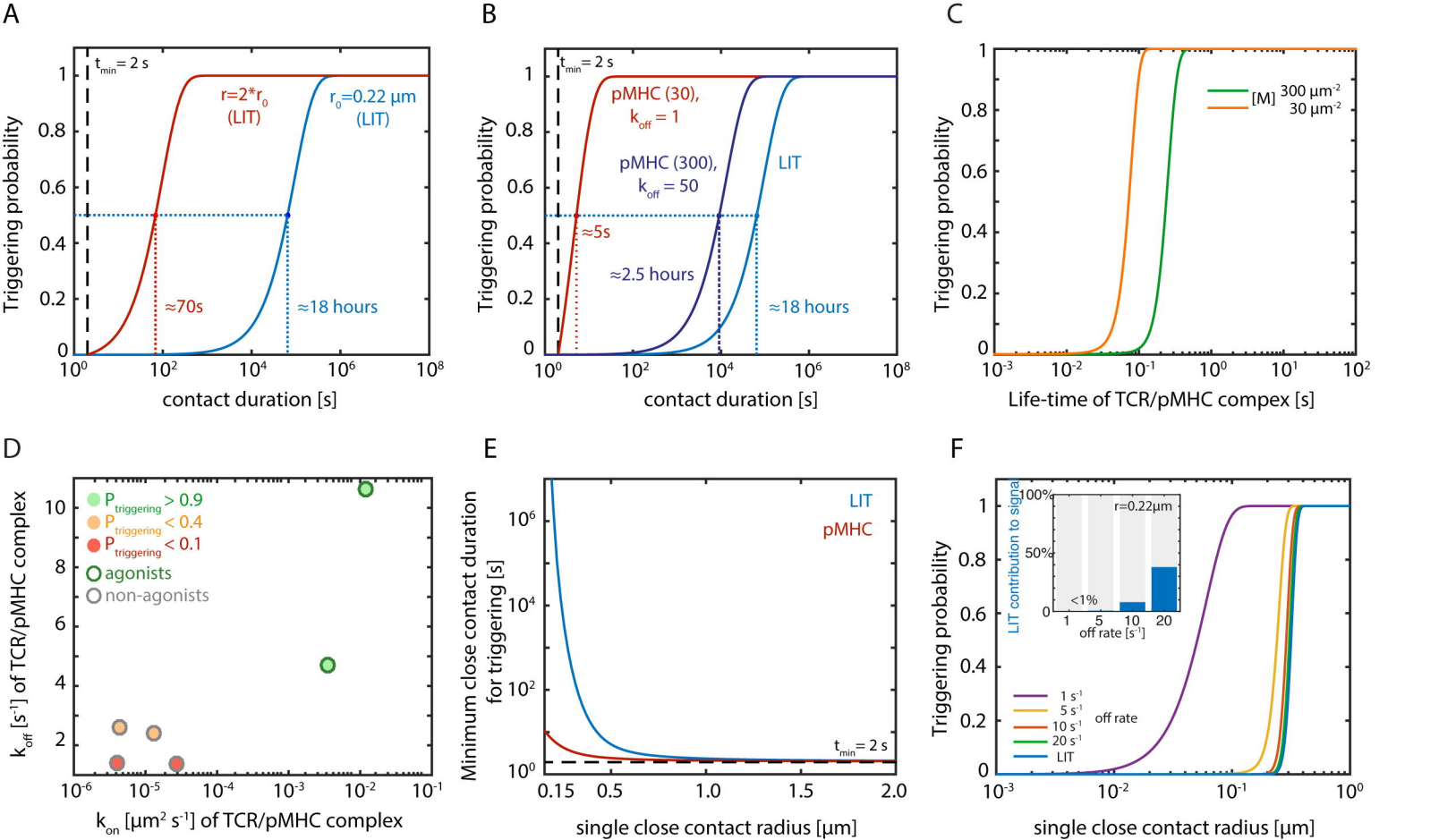
A
B
C
D
E
F
Triggering probability
contact duration [s]
t_{min} = 2 s
r=2*r_0 (LIT)
r_0=0.22 µm (LIT)
≈70s
≈18 hours
pMHC (30), k_{off} = 1
pMHC (300), k_{off} = 50
LIT
≈5s
≈2.5 hours
[M] 300 µm^{-2} 30 µm^{-2}
Life-time of TCR/pMHC compex [s]
$P_{triggering}$ > 0.9
$P_{triggering}$ < 0.4
$P_{triggering}$ < 0.1
agonists
non-agonists
k_{off} [s^{-1}] of TCR/pMHC complex
k_{on} [µm^2 s^{-1}] of TCR/pMHC complex
Minimum close contact duration for triggering [s]
LIT
pMHC
single close contact radius [µm]
LIT contribution to signal
r=0.22µm
<1%
off rate [s^{-1}]
1 s^{-1}
5 s^{-1}
10 s^{-1}
20 s^{-1}
LIT
off rate

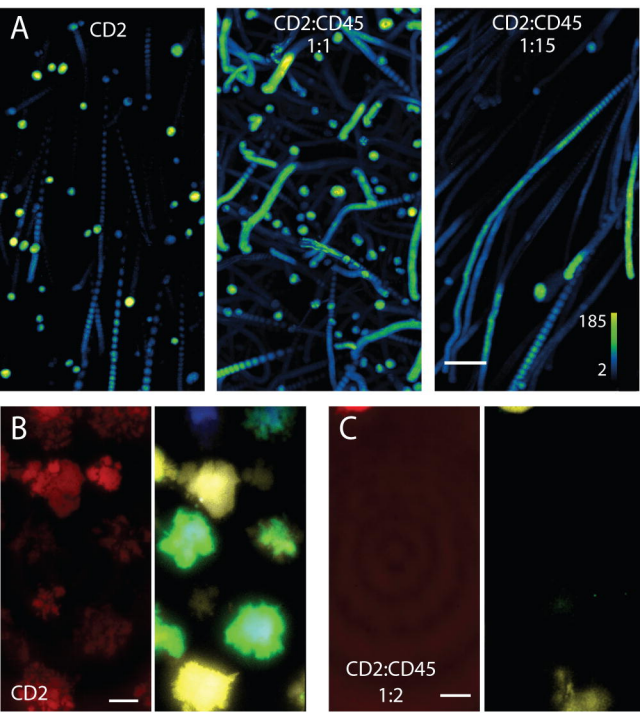
A
CD2
CD2:CD45
1:1
CD2:CD45
1:15
185
2
B
CD2
C
CD2:CD45
1:2

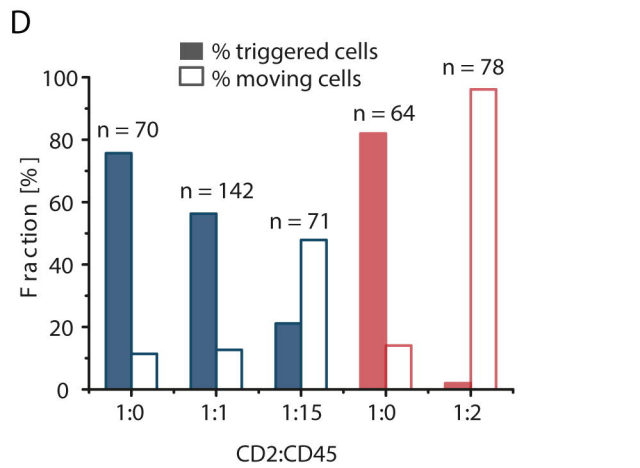
D
% triggered cells
% moving cells
Fraction [%]
100
80
60
40
20
0
n = 70
n = 142
n = 71
n = 64
n = 78
1:0
1:1
1:15
1:0
1:2
CD2:CD45

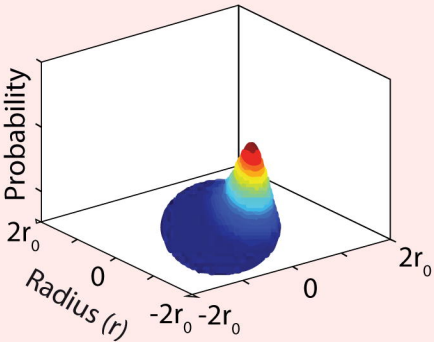

1

The model relies only upon calculation of TCR "dwell-times" at CD45-depleted close-contacts as contact radius (r) increases

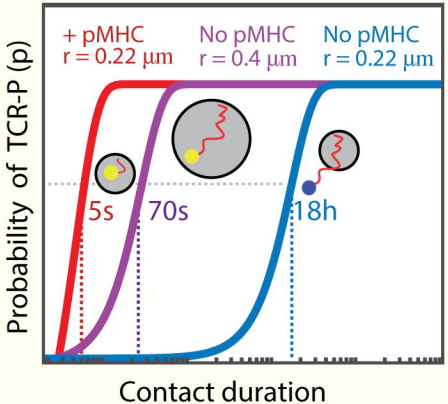

2

It predicts that probability of TCR phosphorylation (p) is affected by close-contact duration and radius, and presence of ligands

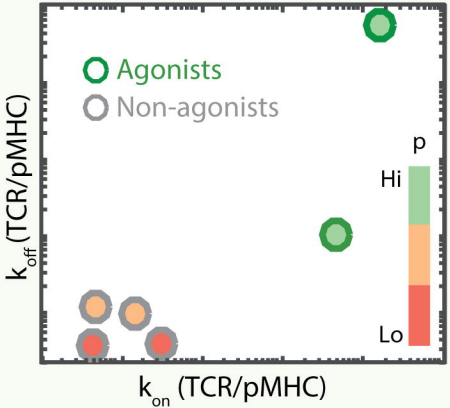

3

A small value for r allows for discrimination between agonists and non-agonists that have known k_{on} and k_{off}